# Fear learning induces α7-nicotinic receptor-mediated astrocytic responsiveness that is required for memory persistence

Kuan Zhang[1,10], Rita Förster[2,3,10], Wenjing He[1], Xiang Liao[4], Jin Li[1], Chuanyan Yang[1], Han Qin[4], Meng Wang[1], Ran Ding[1], Ruijie Li[1,5], Tingliang Jian[1], Yanhong Wang[1], Jianxiong Zhang[1], Zhiqi Yang[1], Wenjun Jin[1], Yonghai Zhang[2,3], Song Qin[6], Yacheng Lu[7], Tao Chen[7,8], Jillian Stobart[9], Bruno Weber[9], Helmuth Adelsberger[2,3], Arthur Konnerth[2,3*], Xiaowei Chen[1,2*]

[1]Brain Research Center and State Key Laboratory of Trauma, Burns, and Combined Injury, Third Military Medical University, Chongqing, China.

[2]Institute of Neuroscience, Technical University of Munich, Munich, Germany.

[3]Munich Cluster for Systems Neurology (SyNergy) and Center for Integrated Protein Sciences (CIPSM), Munich, Germany.

[4]Center for Neurointelligence, School of Medicine, Chongqing University, Chongqing, China.

[5]Advanced Institute for Brain and Intelligence, Guangxi University, Nanning, China.

[6]Department of Anatomy, Histology and Embryology, Shanghai Medical College, Fudan University, Shanghai, China.

[7]Department of Anatomy, Histology & Embryology, Air Force Medical University, Xi'an, China.

[8]Center for Neuron and Disease, Frontier Institute of Science and Technology, Xi'an Jiaotong University, Xi'an, China.

[9]Institute of Pharmacology and Toxicology, University of Zurich and Neuroscience Center Zurich, Eidgenössische Technische Hochschule (ETH) Zurich, Switzerland.

[10]These authors contributed equally to this work.

*Correspondence: arthur.konnerth@tum.de (A.K.); xiaowei_chen@tmmu.edu.cn (X.C.)

**Memory persistence is a fundamental cognitive process for guiding behaviors and considered to rely mostly on neuronal and synaptic plasticity. Whether and how astrocytes contribute to memory persistence has remained largely unknown. Here, by using two-photon $Ca^{2+}$ imaging in head-fixed mice and fiber photometry in freely moving mice, we show that aversive sensory stimulation activates α7-nicotinic receptors in a subpopulation of astrocytes in the auditory cortex. We demonstrate that fear learning causes the *de novo* induction of sound-evoked $Ca^{2+}$ transients in these astrocytes. The astrocytic responsiveness persisted over days along with fear memory and disappeared in animals that underwent extinction of the learned freezing behavior. Conditional genetic deletion of α7-nicotinic receptors in astrocytes significantly impaired fear memory persistence. We conclude that learning-acquired α7-nicotinic receptor-dependent astrocytic responsiveness is an integral part of the cellular substrate underlying memory persistence.**

Memory persistence, or remembering, refers to a systematic process of making information permanently stored and cataloged in the brain so that the information can be retrieved on request[1]. This fundamental cognitive process plays a central role in guiding behaviors that are essential for survival[2] and is often impaired in neurological disorders such as Alzheimer's disease or traumatic brain injury[3]. Previous studies have extensively focused on the role of neurons in memory persistence. It has been suggested that memory persistence involves the replay of the neuronal activity pattern that is present at encoding[4, 5]. To increase the probability that the specific activity pattern reemerges later, memory persistence requires the strengthening or weakening of the synaptic connectivity within participating neuronal ensembles[4, 6]. Therefore, any factors that can change the synaptic connectivity strength of particular neuronal networks may affect memory persistence[1].

Accumulating experimental evidence indicates that glial cells are significant regulators of synaptic function and plasticity[7, 8]. Astrocytes, a major class of glial cells, are able to respond to neuronal activity with intracellular $Ca^{2+}$ transients and then release gliotransmitters that in turn modify synaptic connectivity[8]. Such mutual neuron–astrocyte interactions lead to the concept of the 'tripartite synapse´, in which astrocytes are considered as being active participants in synaptic processing[8]. Astrocytes express different types of neurotransmitter receptors, including noradrenergic, glutamatergic and cholinergic receptors[9]. Through these receptors, astrocytes in the central nervous system respond to various sensory stimuli, including smell, light, sound, tactility and pain[10, 11, 12, 13]. These astrocytic signals not only modulate synapse formation, transmission and plasticity[8, 14, 15], but also regulate the synchronization of neuronal population activity[16]. Thus, through a multiscale regulation of neuronal activity during external sensory stimulation, astrocytes are in an ideal position for contributing to memory formation and persistence[8, 17].

Indeed, astrocytes have been repeatedly shown to be involved in neuronal plasticity both *in vitro*[14, 15] and *in vivo*[13, 18]. Furthermore, a growing body of studies revealed the necessity of astrocytes in normal memory functions *in vivo*[19, 20, 21, 22]. These studies showed that interfering with astrocytic activity resulted in memory impairments. In addition, recent studies showed that adding human astrocytes to the mouse brain[23] or artificially activating astrocytes[24] can cause memory enhancement. However, it has remained unknown whether and how memory-related astrocytic activity changes during information acquisition and storage, owing to difficulties in identifying functionally-defined astrocytes *in vivo* and monitoring their activity in behaving animals across different learning stages over many days. Such investigations would provide the cellular substrate by which astrocytes interact with neurons and contribute to memory formation and persistence.

Fear memory can remain intact for the entire lifetime[5]. Recent studies indicate that astrocytes contribute to the initial stages of fear memory acquisition and consolidation[19, 20, 21, 22, 24]. The artificial activation of astrocytes by chemogenetic manipulations in the CA1 region of the hippocampus can enhance fear memory acquisition[24], but may reduce fear expression in the medial subdivision of the central amygdala[20]. In addition, in the auditory cortex, fear learning has been shown to involve neuronal plasticity[25, 26] and to depend on the recruitment of α7-nicotinic acetylcholine receptor (α7-nAchR)-mediated activation of disinhibitory neuronal circuits[26, 27]. However, it is unknown whether astrocytes in the auditory cortex are involved in the process of fear memory formation and persistence.

In this study, we interrogated the role of cortical astrocytes in memory formation and persistence by using two-photon $Ca^{2+}$ imaging in head-fixed mice[9, 28], optical fiber-based recording in freely moving mice[29, 30] and astrocyte-specific ablation of α7-nAchRs in an auditory associative fear learning task. We discovered a *de novo* induced astrocytic responsiveness mediated by sensory stimulation-activated α7-nAchRs in the auditory cortex during fear memory formation. This responsiveness persisted along with the fear memory behavior over days and ended with its experimentally-induced extinction. Specifically blocking this astrocytic responsiveness impaired memory persistence. Therefore, we suggest that α7-nicotinic receptor-activated astrocytes in the mammalian auditory cortex are essential for the persistence of fear memory.

## Results

### Footshock activates astrocytes in the auditory cortex

We started our study by determining the activity patterns of astrocytes in layers 1 (L1) and 2/3 (L2/3) of the auditory cortex that were stained with the $Ca^{2+}$ indicator fluo-8 acetoxymethyl ester (fluo-8AM) by using a bulk-loading approach[9, 28] (Fig. 1a and Supplementary Fig. 1a). With our adapted protocol (see Methods), an effective astrocytic labeling with fluo-8AM was obtained in a larger region of the auditory cortex, including the primary auditory cortex (Au1), the ventral secondary auditory cortex

(AuV) and a part of the adjacent temporal association cortex (TeA). The specificity of astrocyte labeling with fluo-8AM was confirmed by additional sulforhodamine 101 (SR-101) staining[31] (Supplementary Fig. 1b). Fig. 1a, b illustrates an experiment in which we monitored the activity of astrocytes within a field of view while delivering either sound stimuli or footshocks to a hindlimb. We first used recording conditions of light anesthesia (< 0.5% isoflurane) that did not cause the blockade of astrocytic $Ca^{2+}$ signals observed at deeper levels of anesthesia[12, 32]. Surprisingly, while in this particular experiment none of the astrocytes tested responded to sound stimulation, 4/8 astrocytes reliably responded with $Ca^{2+}$ transients to footshock stimulation ('responders'). Results obtained from similar experiments in 15 animals (189 cells) confirmed these observations by showing that a large fraction of astrocytes was responsive to footshock but only a small minority to sound stimulation (details below). To further verify these results with a sensor suited for longitudinal experiments, we expressed the genetically-encoded $Ca^{2+}$ indicator GCaMP6s[33] specifically in astrocytes of the auditory cortex by injecting the adeno-associated viral construct (AAV)-sGFAP-GCaMP6s[34, 35]. Fig. 1c, d present results indicating that GCaMP6s-stained astrocytes had a similar response pattern as those stained with fluo-8AM. Across all recordings obtained with these two $Ca^{2+}$ sensors, about 64% of the astrocytes (a total of 328 cells in 25 animals tested consisting of 189 cells/15 mice for fluo-8AM and 139 cells/10 mice for GCaMP6s) reliably responded with $Ca^{2+}$ transients to footshock stimulation, while only 8% responded to sound stimulation (Fig. 1e; see example of sound-evoked astrocytic responses in Extended Data Fig. 1). As a caveat we mention that we have no direct confirmation on the status of neuronal activity. Nevertheless, we stress that similar sound stimulation is well known to effectively activate large groups of neurons in the auditory cortex[36, 37, 38, 39, 40]. The footshock-evoked astrocytic $Ca^{2+}$ transients occurred at a relatively large range of latencies after the stimulus (Fig. 1f), similarly to sensory stimulation-evoked astrocytic responses detected in other sensory cortex regions[11, 12].Footshock-evoked astrocytic responses were not restricted to the auditory cortex but observed in other cortical regions, for example in the somatosensory cortex (Supplementary Fig. 2). Together, these results establish that footshock, but not sound, represents a reliable stimulus for the activation of cortical astrocytes.

Multiple lines of evidence from *in vitro* and *in vivo* studies indicate that astrocytic $Ca^{2+}$ transients are often mediated by the activation of $G_q$-coupled neurotransmitter receptor-driven $Ca^{2+}$ release from intracellular endoplasmic reticulum (ER) $Ca^{2+}$ stores[18, 41]. Consistent with those earlier observations, we found that footshock-evoked $Ca^{2+}$ transients were suppressed by the sarco/endoplasmic reticulum $Ca^{2+}$-ATPase (SERCA) antagonist cyclopiazonic acid (CPA) (Fig. 1g, h) or thapsigargin (Fig. 1h and Extended Data Fig. 2a), both known to deplete ER $Ca^{2+}$ stores. Furthermore, application of ryanodine (Fig. 1h and Extended Data Fig. 2b) largely suppressed footshock-evoked responses, indicating an involvement of ryanodine receptors[41]. As demonstrated in a number of previous studies[9, 12, 13, 32, 42, 43, 44], such astrocytic $Ca^{2+}$-induced $Ca^{2+}$ release signals recorded in cell bodies occurred at relatively long

latencies following sensory stimulation (Fig. 1f), in contrast to the short latency signals that can be recorded at the more remote microdomains of the astrocytic processes, the presumed sites of synaptic interaction[34]. Anesthesia was not a relevant determinant for the prolonged delays (anaesthetized mice: 3.1 ± 0.2 s, n = 5 mice versus awake mice: 2.7 ± 0.1 s, n = 4 mice; *P* = 0.2264, two-sided Wilcoxon rank-sum test; Extended Data Fig. 3).

## α7-nAChR-mediated activation of auditory cortex astrocytes

Unlike the spontaneous astrocytic $Ca^{2+}$ waves in the hippocampus *in vivo* that require gap junction-dependent glia-to-glia communication[45], footshock-evoked $Ca^{2+}$ transients were largely insensitive to the gap junction inhibitor carbenoxolone (Extended Data Fig. 2c, d; *n* = 22 cells, 4 mice). Instead, the astrocytic $Ca^{2+}$ transients were completely abolished in 5/5 experiments by the $Na^+$ channel antagonist tetrodotoxin (TTX) that was focally applied to the tested astrocytes (Extended Data Fig. 2e-g; *n* = 55 cells, 5 mice). These experiments indicate that footshock-evoked $Ca^{2+}$ transients in the astrocytes of the auditory cortex are dependent on afferent neuronal activity, without a detectable contribution through gap-junctional activation by other astrocytes.

Since footshock stimulation is known to activate via cholinergic afferents from the basal forebrain many cortical regions, including the auditory cortex[26, 27], we performed pharmacological manipulations with cholinergic and other receptor antagonists under visual guidance using two-photon imaging *in vivo*. The drugs tested were locally applied to the target regions in the auditory cortex using glass pipettes that also contained for better visualization the pharmacologically inert fluorescent dye Alexa Fluor 594. We found that the nicotinic acetylcholine receptor (nAChR) antagonist methyllycaconitine (MLA) abolished completely, and fully reversibly, the $Ca^{2+}$ transients evoked by footshock stimulation (Fig. 2a, b, e). In contrast, neither the muscarinic AChR (mAChR) antagonist VU0255035 (Fig. 2e and Extended Data Fig. 2h) nor a combination of the metabotropic glutamate receptor (mGluR) antagonists MPEP (mGluR5 antagonist) and LY367385 (mGluR1 antagonist; Fig. 2e and Extended Data Fig. 2i) nor ionotropic glutamate receptor antagonists (APV and CNQX) (Fig. 2e and Extended Data Fig. 2j) were effective. Earlier studies have shown that a startle response[43, 46] or a high vigilance state[47] can evoke astrocytic $Ca^{2+}$ transients through norepinephrine-mediated activation of α-adrenergic receptors in the neocortex. However, in our recordings in the auditory cortex obtained at both awake and anesthetized states, footshock-evoked astrocytic $Ca^{2+}$ transients were insensitive to the α-adrenergic receptor antagonist phentolamine (Fig. 2e, Extended Data Fig. 4a, b) or the α1-adrenergic receptor antagonist prazosin (Extended Data Fig. 4c, d). These findings are in clear in contrast to the antagonistic effects of these drugs on startle responses or on vigilance states[43, 46, 47].

The specific role of nAChRs was further substantiated by the observation that all astrocytes that responded to footshock stimulation ('responders') also responded with $Ca^{2+}$ transients to directly

applied nicotine (delivered in the presence of TTX to prevent contributions of nearby neurons, *n* = 69 cells tested; Fig. 2c, d, f). Furthermore, these astrocytes expressed α7-nAChRs (Extended Data Fig. 5). Instead, most 'non-responders' could not be activated by nicotine (Fig. 2f). Finally, we used immunostaining experiments to demonstrate the presence of nAChR α7 subunit-specific puncta on GFAP-positive processes of auditory cortex astrocytes (Fig. 2g)[9].

## Fear learning-induced astrocytic responsiveness to sound

To investigate whether fear learning has any impact on the activity of astrocytes, we next performed *in vivo* two-photon $Ca^{2+}$ imaging experiments in head-fixed, lightly anaesthetized mice before, during and after the presentation of conditioning paired tone/footshock stimuli. After screening different pure tone and complex sound stimulation patterns, known to be differently effective in different auditory cortex subregions[25, 27, 40], we identified a pure tone stimulation protocol (see Methods) as being most effective under our experiment conditions. Also, instead of the standard protocol of 3-5 tone/footshock pairings used in non-anesthetized animals[5, 27], we needed in the lightly anaesthetized animals 10-15 pairings for the induction of long-lasting fear memory. We confirmed that this protocol was indeed effective by showing that the freezing behavior tested later during wakefulness was similar, in terms of strength and persistence, to that observed after conditioning in freely moving animals (see below in Fig. 6b versus Supplementary Fig. 6).

In the experiment illustrated in Fig. 3a-c, we illustrate the changes in 5 astrocytes that initially produced $Ca^{2+}$ transients in response to pure footshock but not in response to pure sound stimuli (Fig. 3b, columns preceding pairing showing one footshock trial and two consecutive sound trials). Fig. 3c illustrates the changes in the $Ca^{2+}$ signaling pattern when delivering repetitively paired stimuli at an interval of 3 min. While pairing #1 evoked a pure footshock-evoked response, we observed already with pairing #3 a trend of astrocytic responsiveness to sound stimuli indicated by the slight upward deflections in the $Ca^{2+}$ trace of cell 1 and cell 5 (blue arrows in Fig. 3c). Within the next 15 pairings, the cells 1, 2, 3 and 5, but not cell 4, developed bona fide sound-evoked $Ca^{2+}$ transients. At the end of the pairing period, $Ca^{2+}$ transients could be evoked just by sound stimuli alone (Fig. 3b, columns following pairing showing two consecutive sound trials and one footshock trial). Similar observations were made in 30/30 astrocytes tested (4 mice; Fig. 3d). Trace fear conditioning stimulation, involving hippocampal-dependent processess[48], was ineffective in inducing astrocytic sound-evoked $Ca^{2+}$ responsiveness (Extended Data Fig. 6). Despite multiple control and conditioning stimuli in ongoing experiments, the amplitudes of footshock-evoked $Ca^{2+}$ transients did not change during repeated stimulation (Fig. 3b last column; Fig. 3d). Remarkably, while there was a highly significant increase in the number of astrocytes with *de novo* induced sound-evoked responsiveness, the number of astrocytes responding to footshock stimulation remained constant. Furthermore, sound responsiveness was acquired only in

those astrocytes ('responders': ~68% versus 5% before conditioning, *n* = 30 cells, 4 mice) that were footshock-responsive, but not in 'non-responders'. Notably, the response amplitudes to sound stimulation after conditioning correlated positively with the corresponding footshock-evoked responses (Fig. 3e), suggesting that an overlapping set of afferent axons underlie the newly-induced astrocytic $Ca^{2+}$ responses.

To explore the contribution of cholinergic inputs to the learned astrocytic responsiveness to sound stimulation, we locally applied the nAChR antagonist MLA and found that it abolished both footshock- and sound-induced astrocytic $Ca^{2+}$ transients (Fig. 3f). Such a blockage effect was observed in 28/28 astrocytes tested in 4 mice (Fig. 3g). Supplementary Fig. 3 shows that the MLA block was fully reversible. We conclude that the nAChR-dependent activation is of critical importance for the new, paired stimulation-dependent activity in astrocytes.

To exclude possible effects of anesthesia, we next performed a new line of experiments entirely in awake behaving mice. For this purpose, we used an optic fiber photometer[29, 30] and implanted chronically the recording tip of a fine optic fiber into the right auditory cortex after AAV-mediated astrocyte-specific GCaMP6f staining (Fig. 4a, left). This arrangement allowed $Ca^{2+}$ recordings that reflected the activity of a small, local cluster of stained cells that were located just in front of the tip of the optic fiber, as established previously by combined two-photon imaging and optical fiber recordings in the same experiment[49]. *Post-hoc* immunostaining confirmed the specificity of GCaMP6f-targeting to astrocytes and indicated the location of the recording sites in the auditory cortex (Supplementary Fig. 4). The right panel of Fig. 4a shows an example recording in which repeated footshock stimuli reliably evoked astrocytic $Ca^{2+}$ transients with comparable amplitudes. This contrasts with repetitive vigilance state-induced astrocytic $Ca^{2+}$ responses that were shown to attenuate rapidly during consecutive stimuli[47]. Fig. 4b presents an example recording performed in the auditory cortex before, during and after the presentation of conditioning paired tone/footshock stimuli. The conditioning stimulation consisted in this wakefulness condition of 3-5 tone/footshock pairings[5, 27]. The population recordings obtained from a small cluster of stained astrocytes in awake, behaving animals (Fig. 4a-g) were strikingly similar to those obtained from single astrocytes by two-photon imaging in head-fixed animals (Fig. 3a-g). Again, we observed a *de novo* induction of sound-evoked astrocytic $Ca^{2+}$ responsiveness associated with fear learning (Fig. 4b, d, e). Remarkably, we observed an induction of sound-evoked astrocytic $Ca^{2+}$ transients following fear conditioning not only in the auditory cortex but also in the hippocampus (CA1 and dorsal hippocampus, dHP) (Extended Data Fig. 7) and in the basolateral amygdala (BLA) (Extended Data Fig. 8a-d), but not in the somatosensory cortex (Extended Data Fig. 8e-h). Thus, fear learning-dependent induction of astrocytic $Ca^{2+}$ responsiveness was not restricted to the auditory cortex but also expressed in those brain regions known to participate in fear learning-dependent sound processing[5, 27]. However, whether α7-nAChRs are also involved in astrocytic

activation in the hippocampus and the BLA has not been addressed in this study and requires future investigation.

In order to test for the specificity of the conditioned stimulus, we used in the standard experiments a train of 8 kHz tone pulses as $CS^+$ and, as a control, a train of 2 kHz tone pulses as $CS^-$. Fear memory retrieval tests were performed with either $CS^-$ or $CS^+$ 1 day or 5-7 days after fear conditioning (Fig. 5a). Consistent with the two-photon imaging results mentioned above in head-fixed animals (Fig. 3b), optic fiber-recorded astrocytic $Ca^{2+}$ transients obtained during wakefulness were also reliably induced by footshock stimulation (Fig. 4a, c and Fig. 5b), but not by sound stimulation before fear conditioning (Fig. 4b, before and 5b). Fig. 5c, d illustrates representative recordings performed at 1 day and at 7 days after conditioning, respectively, showing that $CS^+$, but not $CS^-$, successfully induced persistent astrocytic $Ca^{2+}$ responsiveness (blue traces in Fig. 5c, d). Similarly to the results obtained under light anesthesia (Fig. 3d), the amplitudes of the footshock-evoked $Ca^{2+}$ transients remained unchanged during repeated stimulation also in the awake animals (Fig. 5e). While $CS^+$ evoked a strong and persistent potentiation of astrocytic $Ca^{2+}$ transients after fear conditioning, $CS^-$ was ineffective (Fig. 5f). The fear learning-induced freezing levels were also significantly higher during $CS^+$ than that during $CS^-$ (Fig. 5g). As an additional control, we reversed in the conditioning experiment the identity of $CS^+$ and $CS^-$ to 2 kHz and 8 kHz stimulation, respectively. As expected from previous observations[40], also 2 kHz tone pulses, as $CS^+$, were highly effective in inducing fear learning (Supplementary Fig. 5). Thus, we conclude that the induction of sound-evoked astrocytic responsiveness was specific to the conditioned stimulus ($CS^+$) but not to the untrained sound stimulus ($CS^-$) that, under other conditions, can cause fear generalization[50].

## Persistence and extinction of the astrocytic responsiveness

While footshock-evoked $Ca^{2+}$ transients were extremely robust over multiple trials of stimulation (e.g. Fig. 3b, c, 4a, and 5b), sound-evoked $Ca^{2+}$ transients were fragile and declined during repeatedly delivered conditioned stimuli (Fig. 4f and 6a). Generally, after 5-10 consecutive sound stimuli, delivered at an interval of 3 min, the sound-evoked astrocytic $Ca^{2+}$ transients were virtually abolished (fiber recordings: $n$ = 6 mice in Fig. 4f; two-photon imaging: $n$ = 80 cells from 6 mice in Fig. 6a). Freezing levels also gradually declined over consecutive sound stimuli (Fig. 4f and Fig. 6b) and were positively correlated with the amplitudes of sound-evoked astrocytic $Ca^{2+}$ transients (Fig. 4g), supporting the notion of a tight and direct link between the astrocytic signaling and the freezing behavior. Nevertheless, while the reduction (or 'extinction') of sound-evoked astrocytic $Ca^{2+}$ responsiveness was nearly complete, a significant component of freezing behavior persisted ($n$ = 6 mice, Fig. 4f, Fig. 6b, c)[5, 27], indicating that the relevant neuronal circuits include astrocyte-independent signaling components.

Previous studies have underscored the contribution of various types of auditory cortex neurons for fear learning and memory[5, 27]. In order to test the long-term correspondence between conditioned sound stimulus-activated astrocytes and fear memory, we delivered the conditioning training stimulation to awake, freely moving animals that were then tested for astrocytic $Ca^{2+}$ signaling at cellular resolution under head-fixed conditions in the two-photon microscope (Fig. 6d). For fear learning induction in the awake state, we used 3-5 pairings and verified with behavioral tests the effectiveness of the stimulation. In control recordings, naïve mice were placed at day 0, the day of conditioning of the test animals, without stimulation in the 'conditioning' box. These control animals were otherwise treated exactly like the test animals. The fraction of astrocytes responding to sound stimulation was very low before fear learning (Fig. 6e, top panel), corresponding to what we had mentioned earlier (Fig. 1e). By contrast, mice that received conditioning training and were tested 1-3 days later had a massive increase in the number of sound-responding astrocytes (Fig. 6e, bottom panel). A similar, persisting increase in sound-responders was observed also 13-15 days post-conditioning (Fig. 6f). Across all experiments, both the fraction of sound-responders and their response strengths were remarkably stable over the period tested of up to 15 experimental days (Fig. 6g, i). Entirely consistent with these results, we found that the conditioned stimulus induced also in awake behaving mice sound-evoked astrocytic $Ca^{2+}$ transients that persisted until the active experimental extinction, for example for least 5-7 days post-conditioning in the experiments illustrated in Fig. 5d, f. After delivering 10 conditioned stimuli to the trained mice, a protocol that causes extinction of the freezing behavior (Supplementary Fig. 6)[5, 27], both the fraction of sound-responding astrocytes and the amplitudes of sound evoked $Ca^{2+}$ transients returned to control levels (Fig. 6h, j). Together, our results demonstrate a remarkably tight link between the conditioned stimulus-dependent astrocytic $Ca^{2+}$ responsiveness and the freezing behavior during fear memory persistence. However, these results do not clarify whether nicotinic activation of astrocytes is directly involved in memory functions or represent just an associated "epiphenomenon".

## Deletion of astrocytic α7-nAChRs impairs memory persistence

In order to explore a possible causal role of astrocyte α7-nicotinic receptors in fear memory persistence, we generated tamoxifen-inducible, time-specific α7-nAChR deficient mice by crossing hGFAP-CreER$^{T2}$ mice[51, 52] with mice having the sequence of the *Chrna7* gene flanked by *loxp* sites (Chrna7$^{loxp/loxp}$) (Fig. 7a, Extended Data Fig. 9a and Supplementary Fig. 7; specificity and efficiency of Cre-mediated recombination in astrocytes in Supplementary Table 1). Like the previous studies that used such hGFAP-CreER$^{T2}$ mice to delete other types of receptors in astrocytes[51, 52], immunostaining control experiments performed after tamoxifen injection (Fig. 7b, c; also see overview images in Extended Data Fig. 9b, c) confirmed the effective deletion of α7-nAChRs in astrocytes in these conditional

knockout mice (cKO; hGFAP-CreER$^{T2}$:Chrna7$^{loxp/loxp}$). In addition, we verified in control experiments involving immuno-electron microscopy (immunoEM) that α7-nAChRs were expressed in cortical astrocytes in cWT mice, but not in cKO mice, while they were present in the neurons of both genotypes (Supplementary Fig. 8). Astrocytes lacking α7-nAChRs were unresponsive to footshock stimulation (Fig. 7d upper, e). A next round of control experiments involved tests of α7-nAChRs in L1 interneurons of the auditory cortex, known to contribute decisively to fear learning[26, 27]. For this purpose, we used immunohistochemistry (Extended Data Fig. 9b, c left and d), *in vivo* electrophysiological (Fig. 7d lower) and two-photon $Ca^{2+}$ imaging recordings (Extended Data Fig. 9f-h). These experiments indicated a normal expression of α7-nAChRs (Extended Data Fig. 9d) as well as the usual nicotine- and footshock-evoked responses in L1 interneurons of cKO mice (Fig. 7d lower, f; Extended Data Fig. 9f-h). After convincing ourselves with these many control experiments that cKO mice lack α7-nAChRs specifically in astrocytes (Fig. 7d upper and e; Extended Data Fig. 9b, c right and e), we performed behavioral tests. We found that cKO mice showed comparable learning abilities during fear conditioning (Fig. 7g), but had significantly reduced fear levels after fear learning as compared to their cWT littermates (hGFAP-CreER$^{T2}$:Chrna7$^{WT/WT}$) (Fig. 7h).

The cKO mice tested above may have deletions of α7-nAChRs not only in the auditory cortex but also in the astrocytes of other brain regions that are involved in some forms of fear learning and memory, such as the hippocampus or the amygdala (Extended Data Fig. 7 and 8a-d). Therefore, to test for the specific contribution of the auditory cortical astrocytes, we performed a region-specific deletion of α7-nAChRs in astrocytes using a viral construct-mediated Cre/lox approach[51]. For this purpose, we bi-laterally injected AAV5-GfaABC$_1$D-Cre[53] into the auditory cortices of adult Chrna7$^{loxp/loxp}$ mice and their cWT littermates (Fig. 8a and Extended Data Fig. 10a). In control experiments, we used immunostaining (Extended Data Fig. 10b-f) and *in vivo* functional analyses including electrophysiology and two-photon $Ca^{2+}$ imaging (Fig. 8b-d and Extended Data Fig. 10g-i) to verify the deletion of α7-nAChRs in astrocytes but the unchanged nicotinic responsiveness of L1 interneurons. Behaviorally, we performed two distinct tests. In the first one, the injection of AAV5-GfaABC$_1$D-Cre into the auditory cortex was performed 3 weeks before fear conditioning (Fig. 8e left). In this situation, the deletion of α7-nAChRs was completed at the time of pairing. While the fear learning process itself was not affected (Fig. 8f), the persistence of the learned fear levels was significantly impaired (Fig. 8g). In the second test, the injection of AAV5-GfaABC$_1$D-Cre into the auditory cortex was performed 24 hours after fear-conditioning but preceded memory retrieval by 3 weeks (Fig. 8e right). Thus, the pairing took place in conditions of an intact function of astrocytic α7-nAChRs and fear learning was unaffected (Fig. 8h). However, fear levels were impaired 3 weeks after the viral construct injection and the associated deletion of astrocytic α7-nAChRs (Fig. 8i). In sum, we conclude that astrocytic α7-nAChRs in the auditory cortex are needed for memory persistence and retrieval.

## Discussion

In the past decades, extensive efforts have been made to investigate the roles of astrocytes in learning and memory. Progress has emerged particularly with the development of advanced methods including genetically-encoded molecular constructs for both targeting and manipulating specifically astrocytes *in vivo*[54]. As a consequence, several recent studies have demonstrated the necessity of astrocytes in various memory functions. Most important are probably insights obtained on the population level showing that interfering with normal astrocyte function can cause memory impairment, while activating them externally can lead to memory enhancement[20, 24]. In the present study, by monitoring astrocyte $Ca^{2+}$ activity on the single cell level over days with *in vivo* two-photon $Ca^{2+}$ imaging and on the level of small clusters with optic fiber-based recordings in freely moving mice, we discovered a new form of learning-induced astrocytic signaling. This occurs in a subset of astrocytes during fear learning, and persists precisely along with the persistence of fear memory and vanishes directly with the extinction of the learned behavior. By using pharmacological, electrophysiological and molecular biological manipulations, we found that this astrocytic responsiveness required activation of α7-nicotinic receptors that were activated by afferent cholinergic neuronal inputs. Genetic deletion of α7-nicotinic receptors specifically in astrocytes of the auditory cortex significantly impaired fear memory persistence. Therefore, the major added value of our study to the field is the identification of a new neuron-glia signaling mechanism in the cortex with a key contribution of these astrocytes to memory persistence. This role of astrocytes had not been anticipated in previous studies[1].

### Neuronal and glial contribution to memory persistence

Memory persistence has been largely attributed to neurons and considered to be due to a persistent change in the function of neurons and circuits based on experience, reflecting what had been transpired at encoding and predicting what can be recovered during retrieval[1]. In the case of auditory associative fear learning, afferent cholinergic inputs were shown to induce long-term modifications of synaptic plasticity in auditory cortex neurons[26, 27]. The long-term plastic modification of the function of cortical afferents to the amygdala is thought to contribute to the persistence of fear memory[5, 25].

However, accumulating experimental evidence indicates that astrocytes can also actively modulate both synaptic transmission and plasticity[7, 8, 18] and ultimately contribute to memory processing[19, 20, 21, 22]. Such astrocytic modulation appears to be both circuit-[55] and stimulus-specific[56]. Our present results indicate that a new form of glial signaling, consisting of learning-acquired $Ca^{2+}$ responsiveness in a subset of cortical astrocytes, can serve as an essential cellular co-substrate of fear memory[5], as it is induced by the conditioned stimulus, persists for many days in tight association with the learned freezing response and vanishes with the extinction of the learned behavior. Importantly, the specific

deletion of this *de novo*-induced astrocytic α7-nicotinic receptor-mediated $Ca^{2+}$ response impairs the learned freezing responses.

**Astrocytic $Ca^{2+}$ responsiveness is α7-nAChR-dependent**

Cholinergic afferents from the basal forebrain to the cortex are classical modulators of cortical neuronal activity and synaptic plasticity, and required for fear learning and memory[5, 26, 27]. Generally, the cholinergic effects are mediated through activation of muscarinic[57] and/or nicotinic receptors[26, 27]. In addition to the well-established roles for neuronal activation and modulation, increasing evidence indicates that cholinergic activation of astrocytes through muscarinic receptors is involved in cortical and hippocampal plasticity[13, 18]. Besides, an expression of α7-nAChRs has been found in astrocytes of different brain regions including the hippocampus and the cortex[9, 54, 58]. *In vitro* recordings have revealed nAChR-mediated $Ca^{2+}$ transients in astrocytes that represent most likely α7-nAChR-mediated signals generated by $Ca^{2+}$-induced $Ca^{2+}$ release from ER stores[41].

Our present results demonstrate that $Ca^{2+}$-induced $Ca^{2+}$ release from ER stores is the signaling mechanism for the sensory stimulation-evoked astrocytic $Ca^{2+}$ responsiveness in the auditory cortex *in vivo*. Furthermore, we identify here for this first time an essential role of nicotinic receptors in cortical astrocytes for learning and memory. We demonstrate that both footshock (US)- and sound (CS)-induced $Ca^{2+}$ transients in cortical astrocytes require α7-nicotinic receptor (α7-nAChR) activation. The astrocyte activation was purely neuronal afferent driven and, thus, different from the previously reported spontaneous astrocytic $Ca^{2+}$ wave activity that required gap junction-dependent glia-to-glia communication[45]. Moreover, unlike the astrocyte activation mechanism observed under a startle or a vigilance condition[43, 46, 47], there was no norepinephrine-mediated contribution to the auditory cortex astrocytic responsiveness during footshock or sound stimulation. Finally, the auditory cortex astrocytic responsiveness also did not require metabotropic glutamate receptors whose activation is involved in the somatosensory cortex astrocytes during whisker stimulation[12]. In summary, the cholinergic neuron-astrocyte circuit of the auditory cortex identified in our study is unique in many of its molecular and functional properties and, well-adapted for fear learning-dependent interactions with the previously-reported nAChR-activated disinhibitory neuronal microcircuit in the auditory cortex[26, 27]. Possibly, while the neuronal microcircuit plays a prime role in the induction of the learning process and behavioral control, learning-induced changes in the astrocytic responsiveness are key factors for fear memory maintenance and persistence.

**Relevance and possible roles of astrocytes for memory**

While glia has a major role in controlling metabolic processes in the brain, a rich previous body of evidence has indicated that astrocytes are also involved in sensory integration and neural plasticity[7, 11,

[12, 18, 20, 54]. The insights obtained in our study demonstrate that astrocytes are not only involved in the dynamic regulation of neuronal responses, but also can play a key role in the prolonged information storage in the brain, especially in conditions like those of fear learning involving activation of large numbers of neurons in the cortex and elsewhere[5]. The contribution of astrocytes may consist in an adaptive control of synaptic processes in the participating neurons[7, 8, 18] as well as metabolic and hemodynamic regulation during the strong freezing behavior-associated increased neuronal activity[11]. As biological processes do not always reach their potential maxima, it is tempting to devise ways to enhance normal memory performance[5, 24]. Here, we demonstrate that astrocytic activity integrates into the stimulus convergence following memory formation and persistence, and ultimately contributes to optimize the memory performance. Considering that artificially manipulating astrocytes by the chemogenetic or optogenetic tool has been proven to be able to promote memory allocation and improve memory performance[24], the requirement of α7-nAChRs in astrocytes for memory persistence revealed in our study may represent an important molecular therapeutic target to fight against cognitive alterations or declines in many central nervous system diseases, such as amnesia, Alzheimer's disease and traumatic brain injury[7, 59].

**Figure legends**

**Fig. 1 | Sensory stimulation-evoked $Ca^{2+}$ signaling in astrocytes of the mouse auditory cortex. a**, Two-photon fluorescence image of fluo-8AM-stained astrocytes in layer 2/3 of the mouse auditory cortex. The imaging depth was 171 µm below the cortical surface. Red arrowheads indicate astrocytes that responded to footshock stimulation ('responders'), while grey arrowheads indicate non-responding cells ('non-responders'). **b**, Sound- and footshock-evoked $Ca^{2+}$ transients (Δf/f) corresponding to the astrocytes indicated in panel **a** (sound stimuli indicated by grey bars; footshock stimuli indicated by red bars). Both single and average (aver.) trials are shown. **c**, **d**, Similar experimental arrangement as in panels **a** and **b** involving the use of GCaMP6s instead of fluo-8AM. The imaging depth was 150 µm. **e**, Pie charts illustrating the fraction of responding and non-responding astrocytes to footshock (left) or sound stimulation (right), respectively ($n$ = 328 cells from 25 mice). **f**, Latency histogram of footshock-evoked $Ca^{2+}$ transients ($n$ = 210 cells). **g**, Footshock-evoked $Ca^{2+}$ transients in 4 representative cells of an imaging plane before, during and after local application of CPA. **h**, Bar graphs summarizing the effects of CPA, thapsigargin, ryanodine or ACSF (artificial cerebrospinal fluid) on the footshock-evoked astrocytic $Ca^{2+}$ transients. The amplitude of $Ca^{2+}$ transients was normalized to the control level (value before drug application). The number of cells tested is indicated on the top of each bar. ***$P$ < 0.001 versus control condition (control versus CPA, $Z$ = 5.5109, $P$ = 3.5694 E-8; control versus thapsigargin, $Z$ = 3.9199, $P$ = 8.8575 E-5; control versus ryanodine, $Z$ = 5.4424, $P$ = 5.2553 E-8; control versus ACSF, $Z$ = -1.0986, $P$ = 0.2719), two-sided Wilcoxon signed-rank test. All data in the figure are shown as mean ± s.e.m..

**Fig. 2 | Nicotinic acetylcholine receptor-dependence of footshock-evoked astrocytic responses. a**, Two-photon image of fluo-8AM-stained astrocytes with the schematic representation of a glass pipette that was used for local MLA application (imaging depth 250 µm). **b**, Footshock-evoked $Ca^{2+}$ transients obtained in the 5 astrocytes indicated in panel **a** before, during, and after MLA application. **c**, **d**, Same arrangement as in panels **a** and **b** but application of ACSF or nicotine (in the presence of TTX, imaging depth 125 µm). **e**, Bar graph summarizing the effects of MLA, VU0255035 (muscarinic AChR antagonist), combination of MPEP and LY367385 (both group I mGluR antagonists), combination of APV and CNQX (iGluR antagonists, ionotropic glutamate receptor antagonists), or phentolamine (α-adrenergic receptor antagonist) on footshock-evoked $Ca^{2+}$ transients. The amplitudes of the $Ca^{2+}$ transients were normalized to control levels (values before drug application). The number of cells is indicated on top of each bar. ***$P$ < 0.001 versus control (control versus MLA, $Z$ = 4.7033, $P$ = 2.5596 E-6; control versus VU0255035, $Z$ = 1.4374, $P$ = 0.1506; control versus MPEP+LY367385, $Z$ = 1.87, $P$ = 0.0615; control versus APV+CNQX, $Z$ = 1.4604, $P$ = 0.1442; control versus phentolamine, $Z$ = 0.1521, $P$ = 0.8791), two-sided

Wilcoxon signed-rank test. **f**, Pie chart illustrating the nicotine-sensitivity (striped area) of cells responding (responders) or not responding (non-responders) to footshock (*n* = 69 cells). **g**, Confocal images of a cortical section of the mouse auditory cortex immunostained for α7 subunit (green, left) and GFAP (red, middle). Similar results were obtained in 13 slices from 3 mice. All data in the figure are shown as mean ± s.e.m..

**Fig. 3 | *De novo* induction of sound-evoked astrocytic responses by fear learning. a**, Two-photon image of a fluo-8AM-stained area in the auditory cortex (imaging depth 269 μm). **b**, Left, $Ca^{2+}$ transients recorded in astrocytes indicated in panel **a** (red traces, "footshock, before") during footshock or sound stimulation (black traces, "sound stim., before"; two consecutive trials) before pairing; right, the sound-evoked responsiveness (blue traces, "sound stim., after"; two consecutive trials) and the footshock-evoked responses ("footshock, after") after pairing. **c**, $Ca^{2+}$ transients during conditioning for selected pairs of sound/footshock stimuli. Note the gradual development of responsiveness to sound stimulation (blue arrows and traces) for cell1, cell2, cell3 and cell5. **d**, Bar graph summarizing the changes in amplitude of astrocytic $Ca^{2+}$ transients in response to sound (blue) or to footshock stimulation (red) before and after conditioning. All amplitudes were normalized to that of the respective initial $Ca^{2+}$ transients produced by footshock (fear conditioning: *n* = 29 cells from 4 mice; before-footshock versus after-footshock, *Z* = 1.7306, *P* = 0.0835; before-sound versus after-sound, *Z* = -4.7030 *P* = 2.5631 E-6; ***$P < 0.001$, two-sided Wilcoxon signed-rank test.). **e,** Plot of sound versus footshock-evoked astrocytic $Ca^{2+}$ transient amplitudes after conditioning. *n* = 29 cells from 4 mice; Spearman *r* = 0.4793, *P* (two tailed) = 0.0092, ** $P < 0.01$. **f**, MLA-dependent blockade of footshock- and sound-evoked responses. The duration of MLA application is indicated by a green bar. **g**, Bar graph summarizing the MLA blockade. The amplitudes of the $Ca^{2+}$ transients were normalized to those of the initial footshock-evoked responses (*n* = 28 cells from 4 mice; control-footshock versus MLA-footshock, *Z* = 4.6227, *P* = 3.7869 E-6; control-sound versus MLA-sound, *Z* = -4.6226, *P* = 3.7896 E-6; ***$P < 0.001$, two-sided Wilcoxon signed-rank test). All data in the figure are shown as mean ± s.e.m..

**Fig. 4 | Fear learning-dependent induction of astrocytic $Ca^{2+}$ responsiveness in awake behaving mice.** **a**, Recording of astrocytic $Ca^{2+}$ signals in freely moving mice by fiber photometry. Left, schematic of the optical fiber recording. Right, footshock-evoked astrocytic $Ca^{2+}$ transients during consecutive trials. **b**, Astrocytic $Ca^{2+}$ transients in response to footshock or sound before, during and after pairing. **c**, **d**, Bar graphs summarizing the amplitudes of astrocytic $Ca^{2+}$ transients in response to footshock (**c**) or sound (**d**) before and after conditioning. *n* = 6 mice in each group (**c**: "footshock-before" versus "footshock-after", *Z* = 0.7338, *P* = 0.4631; **d**: "sound-before" versus "sound-after", *Z* = -2.2014, *P* = 0.0277; *$P <$

0.05, two-sided Wilcoxon signed rank test). **e,** Summary of the freezing levels before and after conditioning. *n* = 6 mice (baseline: before versus after, *Z* = -0.9540*, P* = 0.3401; CS: before versus after, *Z* = -2.2014*, P* = 0.0277; **P* < 0.05, two-sided Wilcoxon signed rank test). **f,** Summary of the decline of the astrocytic $Ca^{2+}$ responsiveness (blue) and freezing levels (green) over multiple sound stimuli after conditioning (*n* = 6 mice). **g,** Correlation between amplitudes of astrocytic $Ca^{2+}$ transients and freezing levels in response to sound after conditioning. *n* = 36 trials from 6 mice; Spearman *r* = 0.7165, *P* (two tailed) = 8.9087 E-7, *** *P* < 0.001. All data in the figure are shown as mean ± s.e.m..

**Fig. 5 | *De novo* induction of sound-evoked astrocytic $Ca^{2+}$ responses by conditioned stimulus ($CS^+$), but not by $CS^-$ in freely moving mice.** **a**, Upper, schematic of optical fiber recording. Lower, fear conditioning protocol. **b**, $Ca^{2+}$ transients recorded in astrocytes responsive initially to footshock (red traces, first column) but not to $CS^-$ or $CS^+$. **c**, **d**, Astrocytic $Ca^{2+}$ transients in response to footshock or $CS^-$/$CS^+$ during pairing and 1 day (**c**) or 7 days (**d**) post-pairing. **e**, **f**, Bar graphs summarizing the amplitudes of astrocytic $Ca^{2+}$ transients in response to footshock (**e**) or $CS^+$/$CS^-$ (**f**) before, 1 day and 5-7 days after conditioning. Footshock: *n* = 8 mice in 'before' group, *n* = 7 mice in 'after 1 d' group, *n* = 6 mice in 'after 5-7 d' group (**e**: "footshock-before" versus "footshock-after 1 d", *Z* = 1.0142*, P* = 0.3105; "footshock-before" versus "footshock-after 5-7 d", *Z* = 0.3145*, P* = 0.7532); $CS^-$/$CS^+$ : *n* = 8 mice in 'before' group, *n* = 6 mice in 'after 1d' and 'after 5-7 d' group (**f**: "$CS^-$-before" versus "$CS^+$-before", *Z* = -1.4003*, P* = 0.1614, "$CS^-$-after 1 d" versus "$CS^+$-after 1 d", *Z* = -2.2014*, P* = 0.0277; "$CS^-$-after 5-7 d" versus "$CS^+$-after 5-7 d", *Z* = -2.2014*, P* = 0.0277; * *P* < 0.05, two-sided Wilcoxon signed rank test). **g**, Summary of the freezing levels to $CS^-$ and $CS^+$. *n* = 8 mice in 'before' and 'after 1d' group, *n* = 6 mice in 'after 5-7d' group (two-way ANOVA; main effect of condition: $F_{2, 57}$ = 353.71, *P* = 7.37 E-33; main effect of day: $F_{2, 57}$ = 128.58, *P* = 7.48 E-22; condition × day interaction: $F_{4,57}$= 81.64, *P* = 6.40 E-23; "baseline after 1 d" versus "$CS^-$ after 1 d": *P* = 0.0095, "baseline after 1 d" versus "$CS^+$ after 1d": *P* = 3.69 E-29, "$CS^-$-after 1 d" versus "$CS^+$-after 1 d": *P* = 4.02 E-25,"baseline after 5-7 d" versus "$CS^-$ after 5-7 d": *P* = 0.0007,"baseline after 5-7 d" versus "$CS^+$ after 5-7 d": *P* = 2.02 E-24,"$CS^-$-after 5-7 d" versus "$CS^+$-after 5-7 d": *P* = 1.40 E-18; ***P* < 0.01, ****P* < 0.001, two-way ANOVA with Bonferroni post hoc comparisons test). All data in the figure are shown as mean ± s.e.m..

**Fig. 6 | Long-term persistence and extinction of the astrocytic responsiveness. a,** 'Extinction' of cellular responsiveness indicated by the gradual disappearance of response to sound during repeatedly delivered CS (*n* = 80 cells from 6 head-fixed, anesthetized mice). **b**, Extinction of freezing behavior in freely running animals (*n* = 6 mice, obtained one day after conditioning). **c,** Comparison of reduction in cellular and behavioral response across CSs ($\sum (CS_n\text{-}CS_{n+1})/\sum CS_n$). *n* = 6 mice in each group (cellular versus behavioral response, *Z* = 2.3259, *P* = 0.02; **P* < 0.05, two-sided Wilcoxon rank sum test). **d**,

Experimental protocol for testing long-term persistence of astrocytic responsiveness. **e**, Top row: two-photon images of fluo-8AM-stained astrocytes from different control mice at days 1 (d1), d2 and d3 after conditioning. Responding cells are indicated by red circles, non-responding ones by grey circles. The right-most panels present superimposed example traces of all tested astrocytes from the images in the corresponding row. The red number indicates the responsive cells, the grey number the non-responsive ones. Bottom row: similar results obtained in conditioned animals. **f**, Same arrangement as in panel **e** showing results obtained at 13-15 days post-conditioning. **g**, The fraction of sound-responsive cells in three control (grey) and three conditioned groups (blue) at different days post-conditioning. The numbers of cells (and mice) are indicated in each bar graph (1-4 days: control versus post-conditioning, Z = -2.9530, *P* = 0.0031; 5-8 days: control versus post-conditioning, Z = -2.9972, *P* = 0.0027; 11-15 days: control versus post-conditioning, Z = -2.9912, *P* = 0.0028; two-sided Wilcoxon rank sum test, ***P* < 0.01). **h**, The fraction of sound-responsive cells in three conditioned groups before (blue, the same as the conditioned groups in panel **g**) and after extinction (black). The numbers of cells (and mice) are indicated in each bar graph (1-4 days: post-conditioning versus extinction, Z = 2.3749, *P* = 0.0176; 5-8 days: post-conditioning versus extinction, Z = 2.2075, *P* = 0.0273; 11-15 days: post-conditioning versus extinction, Z = 2.2014, *P* = 0.0277; two-sided Wilcoxon signed rank test, **P* < 0.05). **i**, The amplitude of astrocytic $Ca^{2+}$ transients in response to sound in three control (grey) and three conditioned groups (blue) at different days post-conditioning. The numbers of cells (and mice) are indicated in each bar graph (1-4 days: control versus post-conditioning, Z = -7.7169, *P* = 1.2 E-14; 5-8 days: control versus post-conditioning, Z = -10.8959, *P* = 1.2 E-27; 11-15 days: control versus post-conditioning, Z = -8.0813, *P* = 6.4 E-16; two-sided Wilcoxon rank sum test, ****P* < 0.001). **j**, The amplitude of astrocytic $Ca^{2+}$ transients in three conditioned groups before (blue, the same as the conditioned groups in panel **i**) and after extinction (black). The numbers of cells (and mice) are indicated in each bar graph (1-4 days: post-conditioning versus extinction, Z = 4.5407, *P* = 5.6 E-6; 5-8 days: post-conditioning versus extinction, Z = 4.7030, *P* = 2.6 E-6; 11-15 days: post-conditioning versus extinction, Z = 5.5786, *P* = 2.4 E-8; two-sided Wilcoxon signed rank test, ****P* < 0.001). All data in the figure are shown as mean ± s.e.m..

**Fig. 7 | Impairment of fear memory persistence by tamoxifen-inducible deletion of α7 subunit of nAChRs in astrocytes. a**, Procedure for the generation of tamoxifen-inducible, astrocyte-specific α7-cKO mice. **b**, **c**, Immunostaining of α7 subunit of nAChRs and of astrocytes (S100β) in the auditory cortex of α7-cWT (**b**) and α7-cKO (**c**). **d**, Upper, footshock-evoked responses in representative cortical astrocytes in α7-cWT (green) and α7-cKO (red). Lower, nicotine-evoked spike responses in representative layer 1 (L1) interneurons in α7-cWT (green) and α7-cKO (red)**. e**, Summary of the footshock-evoked responses in astrocytes. n = 11 fields of view (97 cells of 4 mice) in cWT group; n =

12 fields of view (118 cells of 4 mice) in cKO group (cWT versus cKO, $Z$ = 4.3566, $P$ = 1.3211 E-5, two-sided Wilcoxon rank-sum test, ***$P$ < 0.001.). **f**, Summary of the nicotine-evoked responses in L1 interneurons (spike frequency; n = 10 of 25 cells from 3 mice in cWT group, n = 9 of 22 cells from 3 mice in cKO group; baseline: cWT versus cKO, $Z$ = 0.0409, $P$ =0.9674; nicotine: cWT versus cKO, $Z$ = 0.5307, $P$ = 0.5956, two-sided Wilcoxon rank-sum test). **g,** Freezing levels of cWT and cKO during fear conditioning ($n$ = 10 mice in cWT group, $n$ = 6 mice in cKO group). **h**, Summary of the freezing levels in both genotypes after fear conditioning (n = 10 mice in cWT group, n = 6 mice in cKO group; baseline: cWT versus cKO, Z = -1.2492, $P$ = 0.2116; CS: cWT versus cKO, Z = 3.1501, $P$ = 0.0016, two-sided Wilcoxon rank sum test, **$P$ < 0.01.). In this figure, the number of tested cells (and mice) is indicated on the top of each bar graph. All data in the figure are shown as mean ± s.e.m..

**Fig. 8 | Impairment of fear memory persistence by auditory cortex-specific deletion of astrocytic α7 subunit of nAChRs. a**, Schematic indicating the sites of bilateral viral injections in the auditory cortex. **b**, Footshock-evoked astrocytic responses (upper) and nicotine-evoked neuronal responses (lower) in cWT (AAV+Chrna7$^{WT/WT}$) and cKO (AAV+Chrna7$^{loxp/loxp}$). **c**, Summary of the footshock-evoked responses in astrocytes. n = 6 fields of view (111 cells from 3 mice) in cWT group; n = 14 fields of view (142 cells from 4 mice) in cKO group (cWT versus cKO, $Z$ = -3.5901, $P$ = 3.3060 E-4, two-sided Wilcoxon rank-sum test, ***$P$ < 0.001). **d**, Summary of the nicotine-evoked responses in L1 interneurons (spike frequency; n = 9 of 21 cells from 3 mice in cWT group, n = 7 of 18 cells from 3 mice in cKO group; baseline: cWT versus cKO, $Z$ = 1.2893, $P$ = 0.1973; Nicotine: cWT versus cKO, $Z$ = -1.1652, $P$ = 0.2439; two-sided Wilcoxon rank-sum test). **e**, Protocols of the fear behavior experiments in virus-induced region-specific astrocytic α7-nAchR conditional knockout mice (AAV+Chrna7$^{loxp/loxp}$, cKO). AAV were respectively injected before (left) and after (right) conditioning. **f,** Freezing levels of cWT and cKO during conditioning (AAV injection before conditioning, $n$ = 10 mice in each group). **g,** Summary of the freezing levels in both genotypes (AAV injection before conditioning, n = 10 mice in each group; baseline: cWT versus cKO, Z= -0.8776, $P$ = 0.3802; CS: cWT versus cKO, Z= 3.1773, $P$ = 0.0015; two-sided Wilcoxon rank sum test, **$P$ < 0.01). **h,** Freezing levels of cWT and cKO during conditioning (AAV injection after conditioning, $n$ = 8 mice in each group). **i**, Summary of the freezing levels in both genotypes (AAV injection after fear conditioning; $n$ = 8 mice in each group; baseline: cWT versus cKO, Z= -0.7412, $P$ = 0.4586; CS: cWT versus cKO, Z= 2.5730, $P$ = 0.0101; two-sided Wilcoxon rank sum test, *$P$ < 0.05). In this figure, the number of tested cells (and mice) is indicated on the top of each bar graph. All data in the figure are shown as mean ± s.e.m..

**References**


1. Richards, B.A. & Frankland, P.W. The Persistence and Transience of Memory. *Neuron* **94**, 1071-1084 (2017).

2. Albo, Z. & Graff, J. The mysteries of remote memory. *Philos Trans R Soc Lond B Biol Sci* **373** (2018).

3. Khan, Z.U., Martin-Montanez, E., Navarro-Lobato, I. & Muly, E.C. Memory deficits in aging and neurological diseases. *Prog Mol Biol Transl Sci* **122**, 1-29 (2014).

4. Tonegawa, S., Morrissey, M.D. & Kitamura, T. The role of engram cells in the systems consolidation of memory. *Nat Rev Neurosci* **19**, 485-498 (2018).

5. Maren, S. & Quirk, G.J. Neuronal signalling of fear memory. *Nat. Rev. Neurosci.* **5**, 844-852 (2004).

6. Bliss, T.V. & Collingridge, G.L. A synaptic model of memory: long-term potentiation in the hippocampus. *Nature* **361**, 31-39 (1993).

7. Santello, M., Toni, N. & Volterra, A. Astrocyte function from information processing to cognition and cognitive impairment. *Nature neuroscience* **22**, 154-166 (2019).

8. Haydon, P.G. & Nedergaard, M. How Do Astrocytes Participate in Neural Plasticity? *Cold Spring Harb. Perspect. Biol.* **7** (2014).

9. Zhang, K. *et al.* Sensory Response of Transplanted Astrocytes in Adult Mammalian Cortex In Vivo. *Cerebral cortex (New York, N.Y. : 1991)* **26**, 3690-3704 (2016).

10. Petzold, G.C., Albeanu, D.F., Sato, T.F. & Murthy, V.N. Coupling of neural activity to blood flow in olfactory glomeruli is mediated by astrocytic pathways. *Neuron* **58**, 897-910 (2008).

11. Schummers, J., Yu, H. & Sur, M. Tuned responses of astrocytes and their influence on hemodynamic signals in the visual cortex. *Science* **320**, 1638-1643 (2008).

12. Wang, X. *et al.* Astrocytic Ca2+ signaling evoked by sensory stimulation in vivo. *Nat. Neurosci.* **9**, 816-823 (2006).

13. Takata, N. *et al.* Astrocyte calcium signaling transforms cholinergic modulation to cortical plasticity in vivo. *J. Neurosci.* **31**, 18155-18165 (2011).

14. Panatier, A. *et al.* Astrocytes are endogenous regulators of basal transmission at central synapses. *Cell* **146**, 785-798 (2011).

15. Henneberger, C., Papouin, T., Oliet, S.H. & Rusakov, D.A. Long-term potentiation depends on release of D-serine from astrocytes. *Nature* **463**, 232-236 (2010).

16. Fellin, T. *et al.* Neuronal synchrony mediated by astrocytic glutamate through activation of extrasynaptic NMDA receptors. *Neuron* **43**, 729-743 (2004).

17. Kol, A. *et al.* Astrocytes contribute to remote memory formation by modulating hippocampal-cortical communication during learning. *Nature neuroscience* **23**, 1229-1239 (2020).

18. Navarrete, M. *et al.* Astrocytes mediate in vivo cholinergic-induced synaptic plasticity. *PLoS Biol.* **10**, e1001259 (2012).

19. Suzuki, A. *et al.* Astrocyte-neuron lactate transport is required for long-term memory formation. *Cell* **144**, 810-823 (2011).

20. Martin-Fernandez, M. *et al.* Synapse-specific astrocyte gating of amygdala-related behavior. *Nature neuroscience* **20**, 1540-1548 (2017).

21. Orr, A.G. *et al.* Astrocytic adenosine receptor A2A and Gs-coupled signaling regulate memory. *Nature neuroscience* **18**, 423-434 (2015).

22. Robin, L.M. *et al.* Astroglial CB1 Receptors Determine Synaptic D-Serine Availability to Enable Recognition Memory. *Neuron* **98**, 935-944.e935 (2018).

23. Han, X. *et al.* Forebrain engraftment by human glial progenitor cells enhances synaptic plasticity and learning in adult mice. *Cell Stem Cell* **12**, 342-353 (2013).

24. Adamsky, A. *et al.* Astrocytic Activation Generates De Novo Neuronal Potentiation and Memory Enhancement. *Cell* **174**, 59-71.e14 (2018).

25. Dalmay, T. *et al.* A Critical Role for Neocortical Processing of Threat Memory. *Neuron* **104**, 1180-1194.e1187 (2019).

26. Guo, W., Robert, B. & Polley, D.B. The Cholinergic Basal Forebrain Links Auditory Stimuli with Delayed Reinforcement to Support Learning. *Neuron* **103**, 1164-1177.e1166 (2019).

27. Letzkus, J.J. *et al.* A disinhibitory microcircuit for associative fear learning in the auditory cortex. *Nature* **480**, 331-335 (2011).

28. Hirase, H., Qian, L., Bartho, P. & Buzsaki, G. Calcium dynamics of cortical astrocytic networks in vivo. *PLoS Biol.* **2**, E96 (2004).

29. Yao, J. *et al.* A corticopontine circuit for initiation of urination. *Nature neuroscience* **21**, 1541-1550 (2018).

30. Qin, H. *et al.* A Visual-Cue-Dependent Memory Circuit for Place Navigation. *Neuron* **99**, 47-55.e44 (2018).

31. Nimmerjahn, A., Kirchhoff, F., Kerr, J.N. & Helmchen, F. Sulforhodamine 101 as a specific marker of astroglia in the neocortex in vivo. *Nat. Methods* **1**, 31-37 (2004).

32. Thrane, A.S. *et al.* General anesthesia selectively disrupts astrocyte calcium signaling in the awake mouse cortex. *Proc Natl Acad Sci U S A* **109**, 18974-18979 (2012).

33. Chen, T.W. *et al.* Ultrasensitive fluorescent proteins for imaging neuronal activity. *Nature* **499**, 295-300 (2013).

34. Stobart, J.L. *et al.* Cortical Circuit Activity Evokes Rapid Astrocyte Calcium Signals on a Similar Timescale to Neurons. *Neuron* **98**, 726-735.e724 (2018).

35. Stobart, J.L. *et al.* Long-term In Vivo Calcium Imaging of Astrocytes Reveals Distinct Cellular Compartment Responses to Sensory Stimulation. *Cerebral cortex (New York, N.Y. : 1991)* **28**, 184-198 (2018).

36. Chen, X., Leischner, U., Rochefort, N.L., Nelken, I. & Konnerth, A. Functional mapping of single spines in cortical neurons in vivo. *Nature* **475**, 501-505 (2011).

37. Rothschild, G., Nelken, I. & Mizrahi, A. Functional organization and population dynamics in the mouse primary auditory cortex. *Nat. Neurosci.* **13**, 353-360 (2010).

38. Li, J. *et al.* Primary Auditory Cortex is Required for Anticipatory Motor Response. *Cerebral cortex (New York, N.Y. : 1991)*, 1-18 (2017).

39. Tischbirek, C.H. *et al.* In Vivo Functional Mapping of a Cortical Column at Single-Neuron Resolution. *Cell reports* **27**, 1319-1326.e1315 (2019).

40. Wang, M. *et al.* Single-neuron representation of learned complex sounds in the auditory cortex. *Nature communications* **11**, 4361 (2020).

41. Sharma, G. & Vijayaraghavan, S. Nicotinic cholinergic signaling in hippocampal astrocytes involves calcium-induced calcium release from intracellular stores. *Proc. Natl. Acad. Sci. USA* **98**, 4148-4153 (2001).

42. Srinivasan, R. *et al.* New Transgenic Mouse Lines for Selectively Targeting Astrocytes and Studying Calcium Signals in Astrocyte Processes In Situ and In Vivo. *Neuron* **92**, 1181-1195 (2016).

43. Bekar, L.K., He, W. & Nedergaard, M. Locus coeruleus alpha-adrenergic-mediated activation of cortical astrocytes in vivo. *Cerebral cortex (New York, N.Y. : 1991)* **18**, 2789-2795 (2008).

44. Ding, F. *et al.* alpha1-Adrenergic receptors mediate coordinated Ca2+ signaling of cortical astrocytes in awake, behaving mice. *Cell Calcium* **54**, 387-394 (2013).

45. Kuga, N., Sasaki, T., Takahara, Y., Matsuki, N. & Ikegaya, Y. Large-scale calcium waves traveling through astrocytic networks in vivo. *J. Neurosci.* **31**, 2607-2614 (2011).

46. Paukert, M. *et al.* Norepinephrine controls astroglial responsiveness to local circuit activity. *Neuron* **82**, 1263-1270 (2014).

47. Oe, Y. *et al.* Distinct temporal integration of noradrenaline signaling by astrocytic second messengers during vigilance. *Nature communications* **11**, 471 (2020).

48. Huerta, P.T., Sun, L.D., Wilson, M.A. & Tonegawa, S. Formation of temporal memory requires NMDA receptors within CA1 pyramidal neurons. *Neuron* **25**, 473-480 (2000).

49. Grienberger, C. *et al.* Sound-evoked network calcium transients in mouse auditory cortex in vivo. *J Physiol* **590**, 899-918 (2012).

50. Ghosh, S. & Chattarji, S. Neuronal encoding of the switch from specific to generalized fear. *Nature neuroscience* **18**, 112-120 (2015).

51. Garcia-Caceres, C. *et al.* Astrocytic Insulin Signaling Couples Brain Glucose Uptake with Nutrient Availability. *Cell* **166**, 867-880 (2016).

52. Kim, J.G. *et al.* Leptin signaling in astrocytes regulates hypothalamic neuronal circuits and feeding. *Nature neuroscience* **17**, 908-910 (2014).

53. Nagai, J. *et al.* Hyperactivity with Disrupted Attention by Activation of an Astrocyte Synaptogenic Cue. *Cell* **177**, 1280-1292.e1220 (2019).

54. Zhang, K. & Chen, X. Sensory response in host and engrafted astrocytes of adult brain in Vivo. *Glia* **65**, 1867-1884 (2017).

55. Martín, R., Bajo-Grañeras, R., Moratalla, R., Perea, G. & Araque, A. Circuit-specific signaling in astrocyte-neuron networks in basal ganglia pathways. *Science (New York, N.Y.)* **349**, 730-734 (2015).

56. Mariotti, L. *et al.* Interneuron-specific signaling evokes distinctive somatostatin-mediated responses in adult cortical astrocytes. *Nature communications* **9**, 82-82 (2018).

57. Froemke, R.C. *et al.* Long-term modification of cortical synapses improves sensory perception. *Nature neuroscience* **16**, 79-88 (2013).

58. Duffy, A.M. *et al.* Acetylcholine alpha7 nicotinic and dopamine D2 receptors are targeted to many of the same postsynaptic dendrites and astrocytes in the rodent prefrontal cortex. *Synapse* **65**, 1350-1367 (2011).

59. Blanco-Suárez, E., Caldwell, A.L. & Allen, N.J. Role of astrocyte-synapse interactions in CNS disorders. *J Physiol* **595**, 1903-1916 (2017).

## Methods

**Mice.** C57BL/6 mice were obtained from Laboratory Animal Center at the Third Military Medical University. C57BL/6N-Chrna7$^{tm1a(EUCOMM)Hmgu}$/H (EM#07778) mice were obtained from European Mouse Mutant Archive. B6.Cg-Tg(hGFAP-Cre/ER$^{T2}$)505Fmv/J (JAX#012849) and B6.Cg-*Gt(ROSA)26Sor*$^{tm14(CAG-tdTomato)Hze}$/J (JAX#007914) mice were ordered from Jackson Laboratories. Male, 8-12-week-old mice were used in this study. Mice were housed on a 12-h light/dark cycle, at 22-25°C and in 50-60% relative humidity with ad libitum access to food and water. All animal experiments were carried out in accordance with regulations of the German animal welfare act and protocols approved by the government of Bavaria, Germany and by the Institutional Animal Care and Use Committee of the Third Military Medical University, China.

***In vivo* two-photon $Ca^{2+}$ imaging of cortical astrocytes.** For two-photon $Ca^{2+}$ imaging experiments, surgery and recordings were performed as described previously [9]. In brief, the mouse was placed onto a warming plate (37 – 38 °C) and anesthetized by inhalation of 1-1.5% isoflurane (Curamed, Karlsruhe, Germany, or RWD Life science, Shenzhen, China) in pure $O_2$. The skin and soft tissues were removed under a dissecting microscope after local application of xylocaine. A custom-made recording chamber was then glued to the skull. A craniotomy (~1 mm × 1 mm) centered on the left auditory cortex (bregma -2.5 mm, 4.5 to 4.9 mm lateral to midline, the coordinates that lead to the dye staining area often covering the primary auditory cortex (Au1), ventral secondary auditory cortex (AuV) and a part of the adjacent temporal association cortex (TeA)[25]), or the left primary somatosensory cortex (begma -0.56 mm, 1.65 mm lateral to midline) was made using a high-speed drill with a small-tip steel burr (0.45 mm in diameter). The craniotomy was filled with 1-1.5% low-melting-point agarose to minimize brain pulsations. After surgery, the mouse was transferred into the recording apparatus and then the anesthesia level was decreased to 0.5% isoflurane in pure $O_2$ (breathing rate was around 120 breaths per minute). The recording chamber was perfused with warm normal artificial cerebrospinal fluid (ACSF) containing (in mM): 125 NaCl, 4.5 KCl, 26 $NaHCO_3$, 1.25 $NaH_2PO_4$, 2 $CaCl_2$, 1 $MgCl_2$, and 20 glucose, pH 7.4, when bubbled with 95% $O_2$ and 5% $CO_2$. The temperature of the mouse was maintained in the range of 36.5- 37.5°C throughout the recording.

The $Ca^{2+}$ indicators Fluo-8AM (21081, AAT Bioquest), Rhod-2AM (R1244, Invitrogen; for Extended Data Fig. 5a) or Cal-520 AM (21131, AAT Bioquest; for Extended Data Fig. 9f and 10g) were used for the bulk-loading procedure that was adapted and further developed based on previous reports[9, 28]. Fluo-8AM, Rhod-2AM or Cal-520 AM were dissolved in dimethylsulfoxide (DMSO) with 20% pluronic F-127 and diluted with the normal ACSF solution to a final concentration of ~0.5 mM. The final solutions of Fluo-8AM or Cal-520 AM were applied locally into the target region by pressure (~400 mbar, 2-4 min) using a glass pipette. One hour was required for dye loading of astrocytes or neurons. For Rhod-

2AM, the final solution was loaded on the exposed area for 10 min, followed by a 30-min wash with ACSF. In some experiments, the exposed area was also loaded with SR-101 by surface application after $Ca^{2+}$ imaging to confirm the specificity of labeling [31].

Two-photon $Ca^{2+}$ imaging of astrocytes was performed with a custom-built two-photon microscope system similar to that was reported previously [9]. In this system, the scanner was mounted on an upright microscope (BX61WI, Olympus, Tokyo, Japan) equipped with a water-immersion objective (40×/0.80 NA, Nikon). Full-frame images were acquired at 40 frames/s by custom-written software based on LabVIEW (National Instruments). The excitation laser wavelength was set at 920 nm for imaging of Fluo-8AM-labeled astrocytes and Cal-520AM labeled neurons or at 825 nm for Rhod-2AM-labeled astrocytes. The average power delivered to the brain was adjusted to 20-50 mW, depending on the imaged depth.

***In vivo* electrophysiology.** Local field potential recordings and cell-attached patch-clamp recordings were obtained with an EPC10 amplifier (HEKA Elektronik, Lambrecht/Pfalz, Germany) under two-photon imaging guidance. The patch pipette solution contained normal ACSF solution with 50 μM Alexa Fluor 594 (Invitrogen, A10438) for local field potential recordings or cell-attached recordings. We used the shadow-patching approach for cell-attached patch-clamp recording of neurons.

**Pharmacological manipulation under two-photon imaging.** For local drug application, a glass pipette filled with a mixture of the pharmacological agent and Alexa Fluor 594 (50 μM) was placed in the field of imaging under two-photon imaging guidance[9]. The resistance of pipette (4-6 MΩ) was continuously monitored before, during and after drug application. The drug and Alexa Fluor 594 were co-released by gentle pressure application (Picospritzer III, General Valve). The drug was injected at the following concentration: 50 μM CPA, 10 μM thapsigargin, 50 μM ryanodine, 100 μM MLA, 100 μM VU0255035, 100 μM MPEP, 200 μM LY367385, 100 μM APV, 100 μM CNQX, 100 μM nicotine, 0.5 μM tetrodotoxin (TTX), 50 μM phentolamine, 200 μM prazosin and 100 μM carbenoxolone.

**Fear conditioning and behavior.** We used an associative fear conditioning paradigm in which a conditioned stimulus (CS, an auditory cue) was paired with the presentation of an unconditioned aversive stimulus (US, a footshock). Conditioned stimuli were 9.9-s trains of pure tone (8 kHz, 70 dB sound pressure level), consisting of 33 square pulses of 50 ms duration with inter-pulse interval of 250 ms. The unconditioned stimulus was footshock for 1 s (0.6 - 1mA). The onset of footshock coincided with the end of the last pulse of sound. The interval between two pairings was 3 min. For the experiments in which fear conditioning was performed under two-photon microscope (e.g. see Fig. 3a-f), we applied footshocks to the hindpaws and presented sound from an electrostatic speaker (ES1,

TDT) placed ~5 cm away from the contralateral ear of the mouse. Fear conditioning, inducing freezing behavior when tested during wakefulness (e.g. Fig. 6), was effectively achieved by presentations of 10 to 15 pairings under anesthesia (0.5-0.8% isoflurane). For the experiments in which fear conditioning was performed during wakefulness, we used a custom-made cage comprising of a 30 × 20 × 20-cm plastic box equipped with stainless-steel shocking floor grids that were connected to a feedback current-regulated shocker (conditioning box). A CCD camera (frame rate 30 Hz) with infrared illumination and an electrostatic speaker were placed on the top and the side wall of the box respectively. Before the day of fear conditioning, mice were handled by the experimenter gently for 5 min per day for 3 days. In addition, on the conditioning day, mice were habituated for 5-10 min on the shocking grids in the cage before pairing. Three to five pairings were delivered with an interval of 3 min for inducing fear conditioning. Mice were returned to their home cages 5 min after pairings. Over 1 to 15 days after conditioning, the mice were subjected to either fear retrieval for the fiber recordings (e.g. Fig. 5) or the behavior tests (e.g. Supplementary Fig. 6) in a different context with non-shocking grids or for two-photon imaging under microscope. All equipment was completely cleaned with ethanol, followed by water rinsing, between sessions.

To test whether the response was specific to the trained $CS^+$ tone, we used $CS^+$ (9.9s trains of pure tone, 50 ms duration for each pulse of sound, 33 pulses; 8 kHz, 70 dB sound pressure level) and $CS^-$ (9.9s trains of pure tone, 2 kHz, 70 dB sound pressure level) tones in the experiments. The $CS^+$ tone was paired with the presentation of an unconditioned aversive stimulus (US, a footshock) during fear conditioning. Three to five pairings were delivered with an interval of 3 min for fear conditioning. The $CS^-$ tone was never paired with a footshock. 1 day or 7 days after fear conditioning, mice were subjected to fear retrieval in the presence of $CS^+$ or $CS^-$ tones for both behavior tests and fiber recordings in a different context with non-shocking grids (Fig. 5). In control experiments, we alternated the identity of $CS^+$ and $CS^-$ tones by using 2 kHz as $CS^+$ and 8 kHz as $CS^-$ (Supplementary Fig. 5). The freezing behavior tests were recorded by an infrared CCD camera and analyzed offline. Mice were considered to be freezing if no movement was detected for a duration of 2 s. The freezing level (Fig. 4-8, Extended Data Fig. 7 and 8, Supplementary Fig. 5 and 6) was expressed as a percentage of time spent freezing[27]. To ensure that our automatic system scores freezing rather than just immobility, we previously compared it with the classical time-sampling procedure during which an experimenter blind to the experimental conditions determined the mice to be freezing or not freezing every 2 s (defined as the complete absence of movement except for respiratory movements). The values obtained by classical time-sampling procedure were 95% identical with the automatic detection system which was therefore used throughout the experimental sessions.

**Virus injection for expression of GCaMP6s or GCaMP6f.** C57BL/6 mice were anesthetized with isoflurane (1–1.5% for surgery in pure $O_2$) and placed in a stereotaxic frame, as described previously[29, 30]. A small vertical incision was made in the skin. The skull directly above the injection site was thinned to allow penetration by a glass micropipette containing adeno-associated virus (pAAV). Both AAV constructs (pAAV9-sGFAP-GCaMP6s[34, 35], AAV5-GfaABC$_1$D-cytoGCaMP6f-SV40 (Cat#AV-5-52925, Penn Vector Core)[24, 53] were injected with a volume of 800nl/site without dilution. The AAV vectors were driven by the astrocyte-specific sGFAP or GfaABC$_1$D promotor (a shorter 681bp GFAP promotor)[53] . We injected with a micropipette using a micromanipulator (H. Saur) that was fixed on a custom-made platform. In steps of 100 µm depth we applied in total 150-300 nl of the viral construct at a rate of 0.1 µl/min. After the injection, the pipette was held in place for 15 min before slowly retracting it from the brain. The scalp incision was closed with tissue adhesive (Vetbond, 3M Animal Care Products), and post-injection analgesics were given to aid recovery. Two-photon imaging experiments or optical fiber-based recordings were performed after ~20 days following viral injection. The GCaMP6 injection sites were chosen according to the aims of the experiments: the auditory cortex (AP -3.10 mm, ML ±3.80 mm, DV -1.30 mm with 20 degree slope below the cortical surface for two photon imaging; AP -2.54 mm, ML ±4.6 mm, DV 0 to -0.9 mm for optic fiber recording[25]), the primary somatosensory cortex (AP -0.56, ML ±1.65, DV -0.3 mm), the CA1 of hippocampus (AP -2.06, ML ±1.60, DV -1.1 mm), the dorsal hippocampus (AP -1.7 mm, ML ±1.8 mm, DV -2.0mm) and the BLA in the amygdala (AP -1.6, ML ± 3.1, DV -5.0mm).

**Optic fiber-based recording in freely moving mice.** For fiber implantation surgery, mice labeled with GCaMP6f were anesthetized with isoflurane, and placed in a stereotactic head frame. An optical fiber (diameter 200 µm, NA 0.48; MFP_200/230/900-0.48, Doric lenses, Quebec City, QC, Canada) was inserted into the location where adeno-associated virus (pAAV) were injected, then fixed on the skull with dental cement (Tetric EvoFlow from Ivoclar Vivadent Corporate). For different aims of the experiments, optic fiber ends were inserted at the following coordinates: the auditory cortex (AP -2.54mm, ML ±4.6 mm, DV -0.2 ~ -0.4 mm)[25], the primary somatosensory cortex (AP -0.56, ML ±1.65, DV -0.3 mm), the CA1 of hippocampus (AP -2.06, ML ±1.60, DV -1.1 mm), the dorsal hippocampus (AP -1.7 mm, ML ±1.8 mm, DV -2.0mm) and the BLA in the amygdala (AP -1.6, ML ± 3.1, DV -5.0mm). Optical fiber-based $Ca^{2+}$ recordings were achieved using a modular fiber-optic device, as described previously[29, 30]. The fluorescent signals were sampled at 2000 Hz with custom-written software based on LabVIEW (National Instrument, USA). The animal behavior was simultaneously monitored with a camera (frame rate 30 Hz) under infrared illumination. Optical fiber recordings started after the 3-day handling of animals (5-min handling per day) by the experimenter. On each recording day, mice were habituated for 5-10 min on the shocking cage before experiments. After the end of fiber recording experiments,

mice were killed for histological verification. After perfusion with 4% paraformaldehyde (PFA) and dehydration with 15% sucrose for one night, the brains were cut into 50 µm slices for imaging with a confocal microscope (Zeiss-LSM 700) or a stereoscope (Olympus) (Supplementary Fig. 4).

**AAV-mediated astrocytic nAchR deletion in auditory cortex.** LoxP-Chrna7 transgenic mice, also known as Chrna7$^{loxp/loxp}$ (C57BL/6N-Chrna7$^{tm1a(EUCOMM)Hmgu}$/H, #EM07778), obtained from European Mouse Mutant Archive, EMMA), were injected with AAV5-GfaABC$_1$D-PI-Cre-SV40 (a gift from Baljit Khakh (Addgene plasmid # 105603 ; http://n2t.net/addgene:105603 ; RRID:Addgene_105603))[53] into the auditory cortex (AP -2.54mm, ML ±4.6 mm, DV -0.8mm)[25]. The AAV vectors were driven by the astrocyte-specific GfaABC$_1$D promotor[53], to excise *loxP* sites by Cre recombination. We performed the subsequent behavioral experiments with these mice 3 weeks after viral injection.

**Transgenic mice and tamoxifen induction.** hGFAP-CreER$^{T2}$:Chrna7$^{loxp/loxp}$ (α7-cKO) transgenic mice were generated by crossing hGFAP-CreER$^{T2}$ transgenic mice (#012849, Jackson Laboratories) [51, 52] with loxP-Chrna7 transgenic mice (Chrna7$^{loxp/loxp}$; #EM07778, European Mouse Mutant Archive). The hGFAP-CreER$^{T2}$:Chrna7$^{WT/WT}$ transgenic mice (α7-cWT) from the same littermates were used as the control group. hGFAP-CreER$^{T2}$: tdTomato$^{loxp/loxp}$ transgenic mice were generated by crossing hGFAP-CreER$^{T2}$ transgenic mice with loxP-tdTomato transgenic mice (#007914, Jackson Laboratories). To excise *loxP* sites by Cre recombination, 5-week-old male mice were administrated tamoxifen once per day (100 mg/kg, i.p.) for 5-8 days. Tamoxifen (Sigma-Aldrich) was dissolved in sunflower oil at a final concentration of 10 mg/ml at 37°C, and then filter sterilized and stored for up to 7 days at 4°C in the dark. All control groups are tamoxifen injected littermate control mice (α7-cWT). We performed experiments with these mice 3 weeks after the last injection of tamoxifen.

**Histology and confocal imaging.** For immunohistochemistry, mice were killed by delivery of an isoflurane overdose or by an intraperitoneal injection of sodium pentobarbital and transcardially perfused with 4% paraformaldehyde. The brains were removed, fixed overnight in 4% paraformaldehyde, and cryoprotected in 30% sucrose. Coronal brain sections (30 µm) were prepared and stained as described[29, 30]. Briefly, sections were blocked at room temperature for 30 minutes in 10% normal goat serum, 1% bovine serum albumin, 0.3% TritonX-100 in PBS and incubated with primary antibodies over night at 4°C (goat anti-GFAP, 1:500, Abcam, Ab53554; rabbit anti-NeuN, 1:500, Abcam, Ab177487; mouse anti-α7-nAchR, 1:300, Sigma, M220; rabbit anti-S100β, 1:500, SYSY, 287003; chicken anti-GFP, 1:500, Abcam, Ab13970). Sections were rinsed in PBS, followed by incubation with secondary antibodies directed against immunoglobulins of the appropriate species coupled to Alexa Fluor 594 and 488 (Invitrogen, 1:500; Jackson ImmunoResearch Labs, 1:200). Images were acquired with a Leica

SP5 confocal microscope equipped with standard filter sets and oil immersion objectives (60×/1.42 and 20×/0.85).

**Immunoelectron microscopy.** hGFAP-CreER$^{T2}$:Chrna7$^{WT/WT}$ (α7-cWT) and hGFAP-CreER$^{T2}$:Chrna7$^{loxp/loxp}$ (α7-cKO) mice were anesthetized with 1% sodium pentobarbital intraperitoneally and perfused transcardially with 20 ml saline, followed by 100 ml ice-cold mixture of 4% paraformaldehyde and 0.75% glutaraldehyde in 0.1 M PB for 40 min. Brains were removed and post-fixed by immersion in the same fixative without glutaraldehyde for 4 h at 4 °C. Serial coronal sections of 50 μm thickness were prepared with a vibratome (Microslicer, DTK-1000, Dosaka EMCO, Japan), and then approximately 18–20 sections, including the auditory cortex region, were collected from each brain. α7-nAChR was detected by immunogold-silver staining. S100β was detected by DAB staining. In brief, sections were treated with blocking buffer 0.05 M Tris-buffered saline (TBS, pH7.4) containing 20% (v/v) normal donkey serum for 40 minutes, and then incubated overnight with mouse anti-α7-nAchR antibodies (1:300, Sigma, M220) and rabbit anti-S100β antibody (1:500, SYSY, 287003) diluted with 0.05 M TBS containing 2% (v/v) normal donkey serum (TBS-NGS). The secondary antibody was anti-mouse Nanogold-IgG Goat anti-mouse IgG antibody (Nanoprobes, 2001, 1:100, Yaphank, New York USA) and Biotin-SP conjugated donkey anti-rabbit IgG antibody (Merck Millipore, AP182B, 1:200, Darmstadt, Hessen, Germany) for 4 h. Silver enhancement was performed in the dark with high-quality (HQ) silver enhancement Kit (Nanoprobes, 2012, Yaphank, USA) for visualization of α7-nAchR immunoreactivity. Before and after the silver enhancement step, sections were rinsed several times with deionized water. Then sections were incubated in the avidin-biotin peroxidase complex (ABC standard kit) for 45 min (1:100 dilution in 0.01 M PBS for each solution). To visualize the reaction product, sections were then incubated in diaminobenzidine (4 mg tablet dissolved in 20 ml 0.5 M Tris-HCL, 2 μl 30% hydrogen peroxide). Immunolabelled sections were then fixed with 1% osmium tetroxide in 0.1 M PB for 40 min, dehydrated in graded ethanol series and then in propylene oxide, and finally flat-embedded in Epon 812 between sheets of plastic. After polymerization, acrylic sheets were then peeled from the polymerized resin, and flat-embedded sections were examined under the light microscope. Three to four sections containing α7-nAchR and S100β immunoreactivity were selected from each brain, trimmed under a stereomicroscope, and glued onto blank resin stubs. Serial ultrathin sections were cut with an Ultramicrotome (UC7, Leica, Germany) using a diamond knife (Diatome) and mounted on formvar-coated mesh grids (6–8 sections per grid). They were then counterstained with uranyl acetate and lead citrate, and observed under a JEM-1400 electron microscope (JEOL, Tokyo, Japan) equipped with a CCD camera (Olympus VELETA, Tokyo, Japan) and its application software (iTEM-EMSIS).

**Data analysis and quantification.** Electrophysiological data were sampled at 50 kHz and filtered at 10 kHz using the PatchMaster software (HEKA, Lambrecht, Germany). Data analyses were done using LabVIEW 2014 (National Instruments), MATLAB 2014a (Math Works) or Igor Pro 5.0 (Wavemetrics) in conjunction with custom-written macros[9]. Astrocytic $Ca^{2+}$ transients were expressed as relative fluorescence changes ($\Delta f/f$), corresponding to the mean fluorescence from all pixels within specified regions of interest, as described previously[9]. To extract fluorescence signals, we visually identified astrocytes and performed the drawing of regions of interest (ROIs) based on fluorescence intensity. The $Ca^{2+}$ signal for each ROI was expressed as $\Delta f/f=(f-f_0)/f_0$, where the baseline fluorescence $f_0$ was estimated as the 25th percentile of the entire fluorescence recording. Astrocytes were defined as 'responders' (Fig.1 and Extended Data Fig.2) when maxima of averaged $Ca^{2+}$ signals from 3 consecutive trials 0-9 s after stimuli were above 3 × s.d. of baseline. Therefore, the 'non-responders' should include the weak responses that were smaller than 3 × s.d. of baseline traces. Fiber-based $Ca^{2+}$ recording data were analyzed according to the previously established procedure[29, 30].

**Statistics and reproducibility.** For all experiments, samples were randomized where appropriate for data collection and analysis. Experiments were repeated multiple times on independent occasions as indicated in the Methods and/or Figure legends. All attempts at replication were successful. For optical fiber-based $Ca^{2+}$ recordings, any mice whose virus injection sites or fiber tip sites were missed were excluded from data analysis. Investigators were blinded to groups for dada collection and analysis. No statistical methods were used to pre-determine sample sizes but our sample sizes are similar to those reported in our previous publications with similar methodology[9, 29, 30]. Data were expressed as mean ± s.e.m.. We used nonparametric statistical tests for comparing central tendencies between two data groups. For paired and unpaired cases, we used the two-sided Wilcoxon signed-rank test and the two-sided Wilcoxon rank-sum test, respectively. Group comparisons were made using two-way ANOVA followed by Bonferroni post hoc tests to control for multiple comparisons. Spearman's correlation was used for calculating the correlation between amplitudes of astrocytic $Ca^{2+}$ transients evoked by sound and footshock stimulation or between amplitudes of astrocytic $Ca^{2+}$ transients and freezing levels in response to sound after fear conditioning. $P < 0.05$ was considered statistically significant. For the representative micrographs of Fig. 7b-c, Extended Data Fig. 2e, 9b-c and 10b-c, and Supplementary Fig. 1b, the experiments were repeated independently in 4-5 mice.

**Data Availability**

Any data generated and/or analyzed during the current study are available from the corresponding author on reasonable request. No data sets that require mandatory deposition into a public database were generated during the current study. Source data underlying Figs. 1–8 and Extended Data Figs. 2-4, 6-10 and Supplementary Figs. 5-6 are available as a Source data file.

**Code Availability**

No unique code was generated in this study.

**Acknowledgements**

We thank Jia Lou for technical assistance. B.W. is a member of the Clinical Research Priority Program Molecular Imaging Network Zurich. This work was supported by the National Key R & D Program of China (2018YFA0109600), the National Natural Science Foundation of China (81771175) and the program of China Scholarship Council (201803170004) to K.Z., the National Natural Science Foundation of China (31925018, 31861143038, 31921003, 81671106) and Chongqing Basic Research grants (cstc2019jcyjjqX0001, cstc2019jcyj-cxttX0005) to X.C., the Deutsche Forschungsgemeinschaft (SFB870), an ERC Advanced Grant to A.K.. X.C. is a member of the CAS Center for Excellence in Brain Science and Intelligence Technology. A.K. is a Hertie Senior Professor of Neuroscience.

**Author contributions**

This work was designed by A.K. and X.C.. The main experiments were performed by K.Z., R.F., W.H., J.L., C.Y., H.Q., M.W., R.D., R.L., T.J., Y.W., J.Z., Z.Y., Y.Z., J.S., B.W., H.A., A.K. and X.C. Immunoelectron microscopy experiments were performed by Y.L. and T.C.. Verification of astrocyte-specific Cre-recombination of hGFAP-CreER$^{T2}$:tdTomato$^{loxp/loxp}$ mice was performed by S.Q.. The data analysis was performed by K.Z., R.F., J.L., C.Y., X.L., H.A. W.J. and X.C. This manuscript was written by A.K., X.C. and K.Z. with input from all coauthors.

**Competing interests**

The authors declare no competing interests.

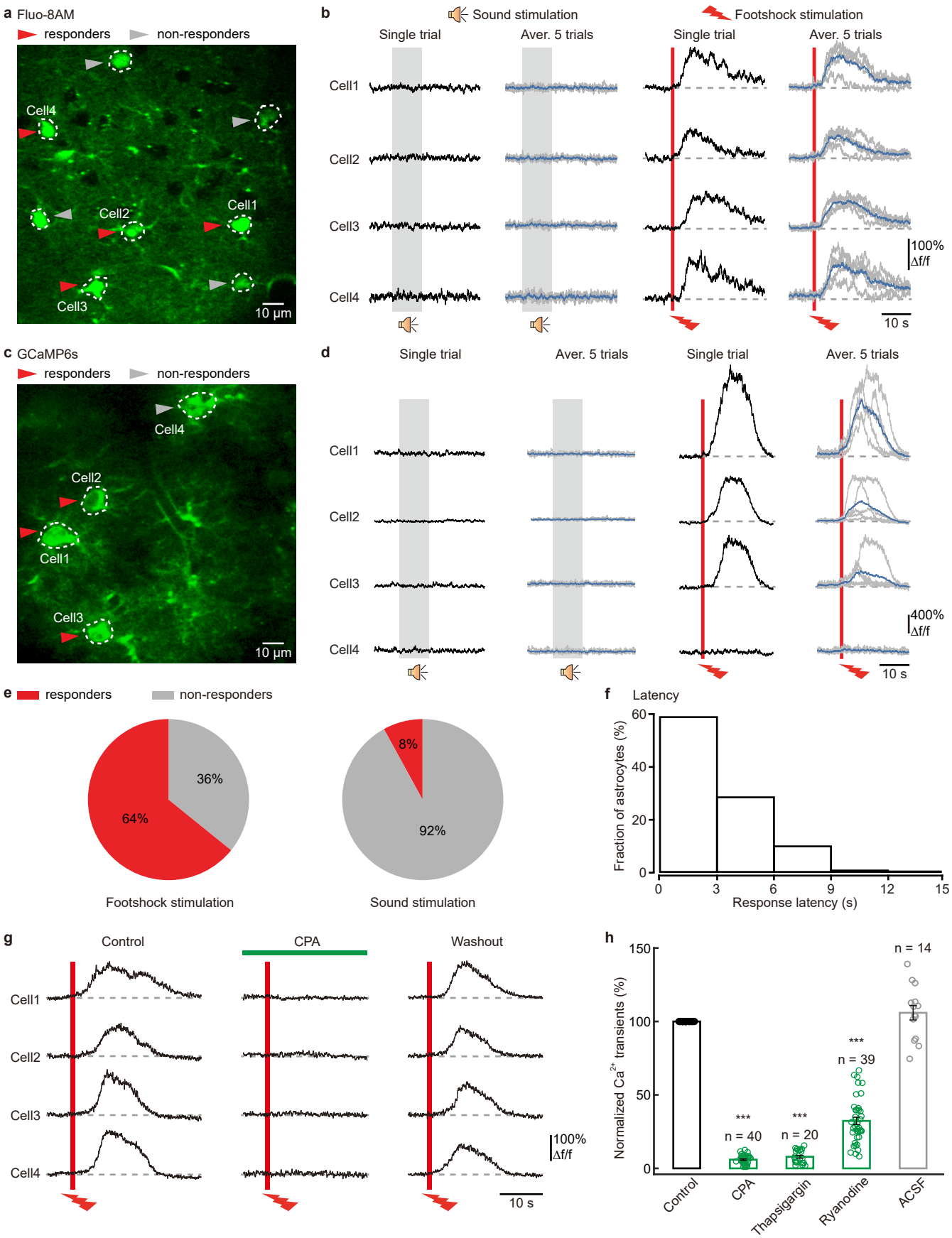
a Fluo-8AM
responders
non-responders
Cell4
Cell2
Cell1
Cell3
10 μm
b
Sound stimulation
Footshock stimulation
Single trial
Aver. 5 trials
Single trial
Aver. 5 trials
Cell1
Cell2
Cell3
Cell4
100%
Δf/f
10 s
c GCaMP6s
responders
non-responders
Cell4
Cell2
Cell1
Cell3
10 μm
d
Single trial
Aver. 5 trials
Single trial
Aver. 5 trials
Cell1
Cell2
Cell3
Cell4
400%
Δf/f
10 s
e
responders
non-responders
36%
64%
Footshock stimulation
8%
92%
Sound stimulation
f
Latency
Fraction of astrocytes (%)
60
40
20
0
0
3
6
9
12
15
Response latency (s)
g
Control
CPA
Washout
Cell1
Cell2
Cell3
Cell4
100%
Δf/f
10 s
h
Normalized Ca2+ transients (%)
150
100
50
0
n = 14
***
n = 39
***
n = 40
***
n = 20
Control
CPA
Thapsigargin
Ryanodine
ACSF

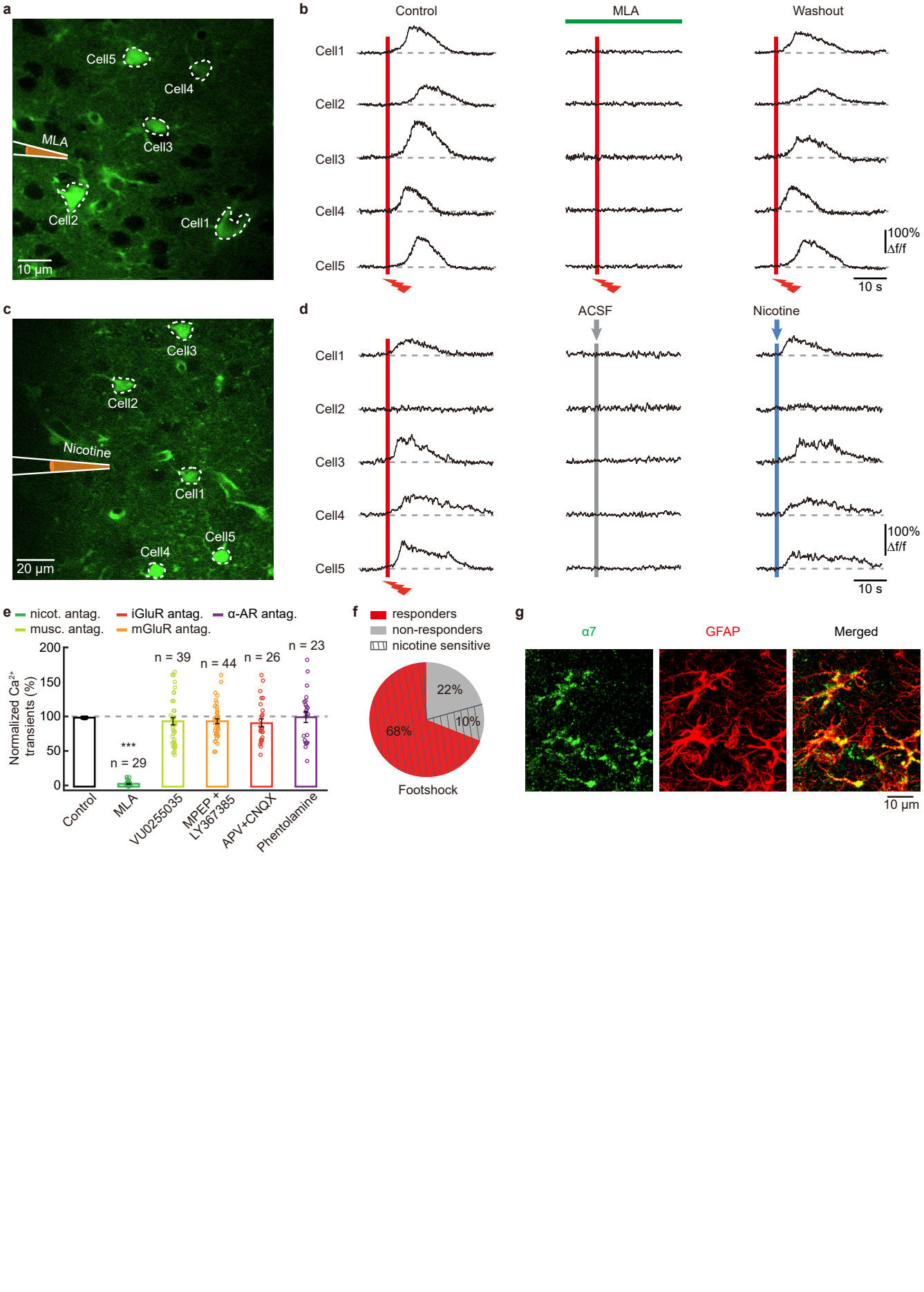
a
Cell5
Cell4
MLA
Cell3
Cell2
Cell1
10 µm
b
Control
MLA
Washout
Cell1
Cell2
Cell3
Cell4
Cell5
100%
Δf/f
10 s
c
Cell3
Cell2
Nicotine
Cell1
Cell5
Cell4
20 µm
d
ACSF
Nicotine
Cell1
Cell2
Cell3
Cell4
Cell5
100%
Δf/f
10 s
e
nicot. antag.
musc. antag.
iGluR antag.
mGluR antag.
α-AR antag.
Normalized Ca2+ transients (%)
200
150
100
50
0
n = 39
n = 44
n = 26
n = 23
***
n = 29
Control
MLA
VU0255035
MPEP + LY367385
APV+CNQX
Phentolamine
f
responders
non-responders
nicotine sensitive
22%
10%
68%
Footshock
g
α7
GFAP
Merged
10 µm

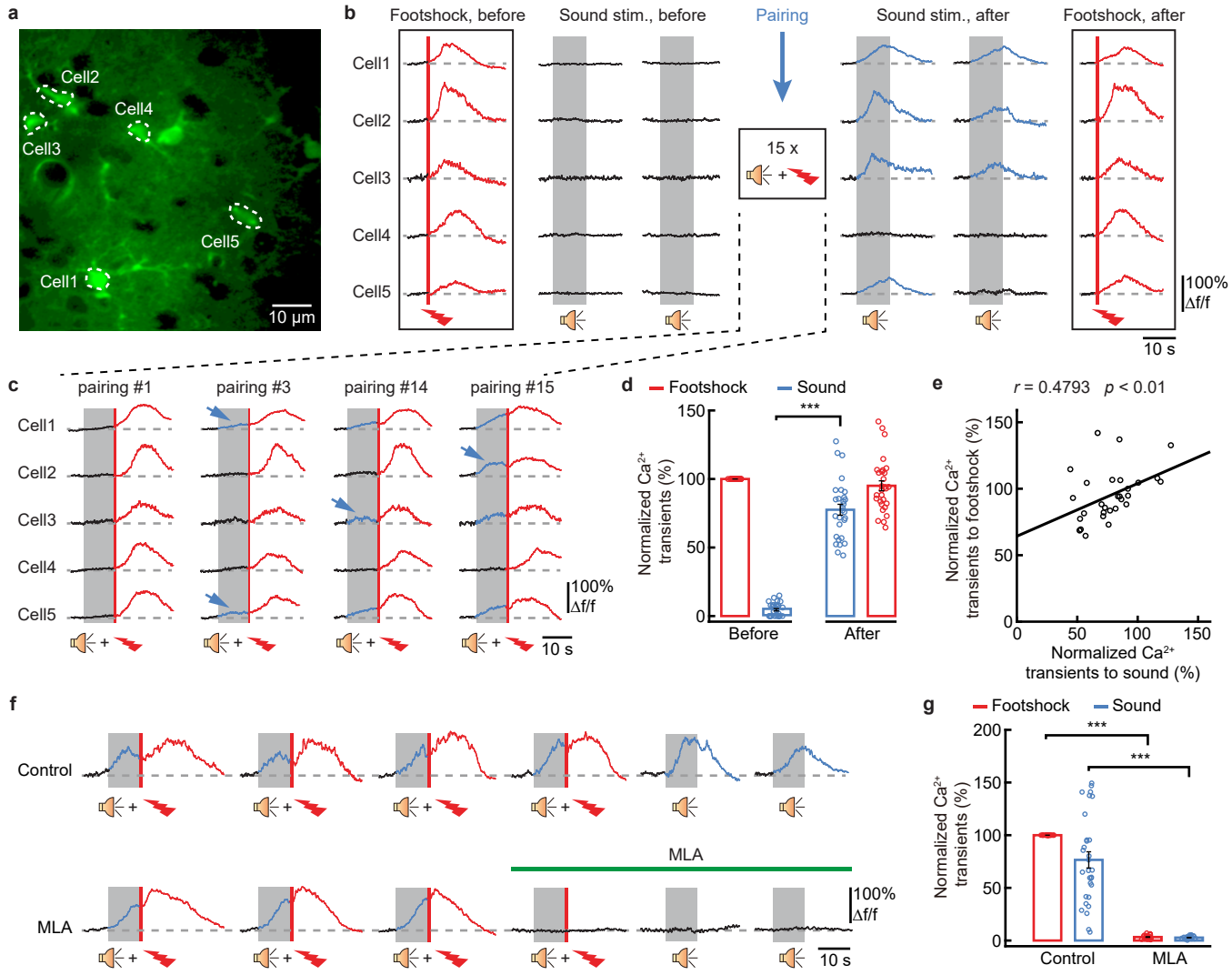
a
Cell2
Cell4
Cell3
Cell5
Cell1
10 μm
b
Footshock, before
Sound stim., before
Pairing
Sound stim., after
Footshock, after
Cell1
Cell2
Cell3
Cell4
Cell5
15 x
100%
Δf/f
10 s
c
pairing #1
pairing #3
pairing #14
pairing #15
Cell1
Cell2
Cell3
Cell4
Cell5
100%
Δf/f
10 s
d
Footshock
Sound
***
Normalized Ca2+ transients (%)
150
100
50
0
Before
After
e
r = 0.4793 p < 0.01
Normalized Ca2+ transients to footshock (%)
Normalized Ca2+ transients to sound (%)
150
100
50
0
0
50
100
150
f
Control
MLA
MLA
100%
Δf/f
10 s
g
Footshock
Sound
***
***
Normalized Ca2+ transients (%)
200
150
100
50
0
Control
MLA

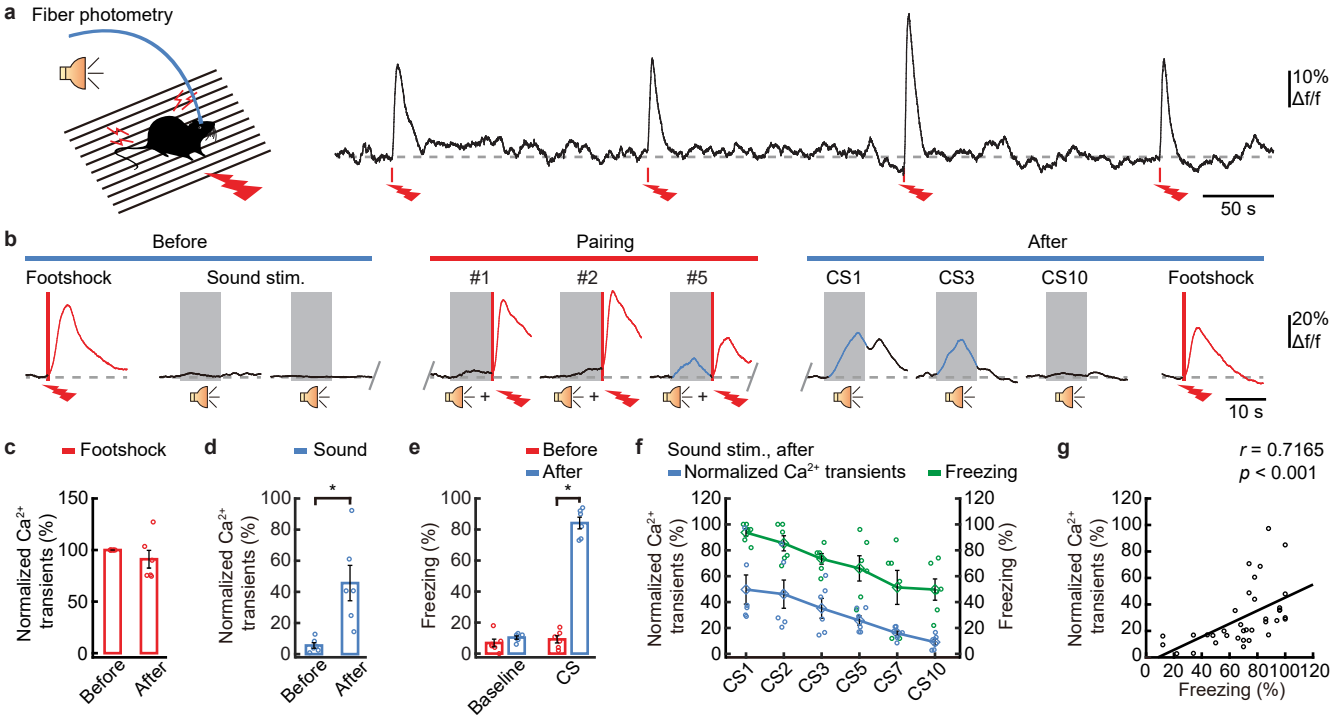
a
Fiber photometry
10%
Δf/f
50 s
b
Before
Pairing
After
Footshock
Sound stim.
#1
#2
#5
CS1
CS3
CS10
Footshock
20%
Δf/f
10 s
c
Footshock
Normalized Ca2+ transients (%)
Before
After
d
Sound
Normalized Ca2+ transients (%)
Before
After
e
Before
After
Freezing (%)
Baseline
CS
f
Sound stim., after
Normalized Ca2+ transients
Freezing
Normalized Ca2+ transients (%)
Freezing (%)
CS1
CS2
CS3
CS5
CS7
CS10
g
r = 0.7165
p < 0.001
Normalized Ca2+ transients (%)
Freezing (%)

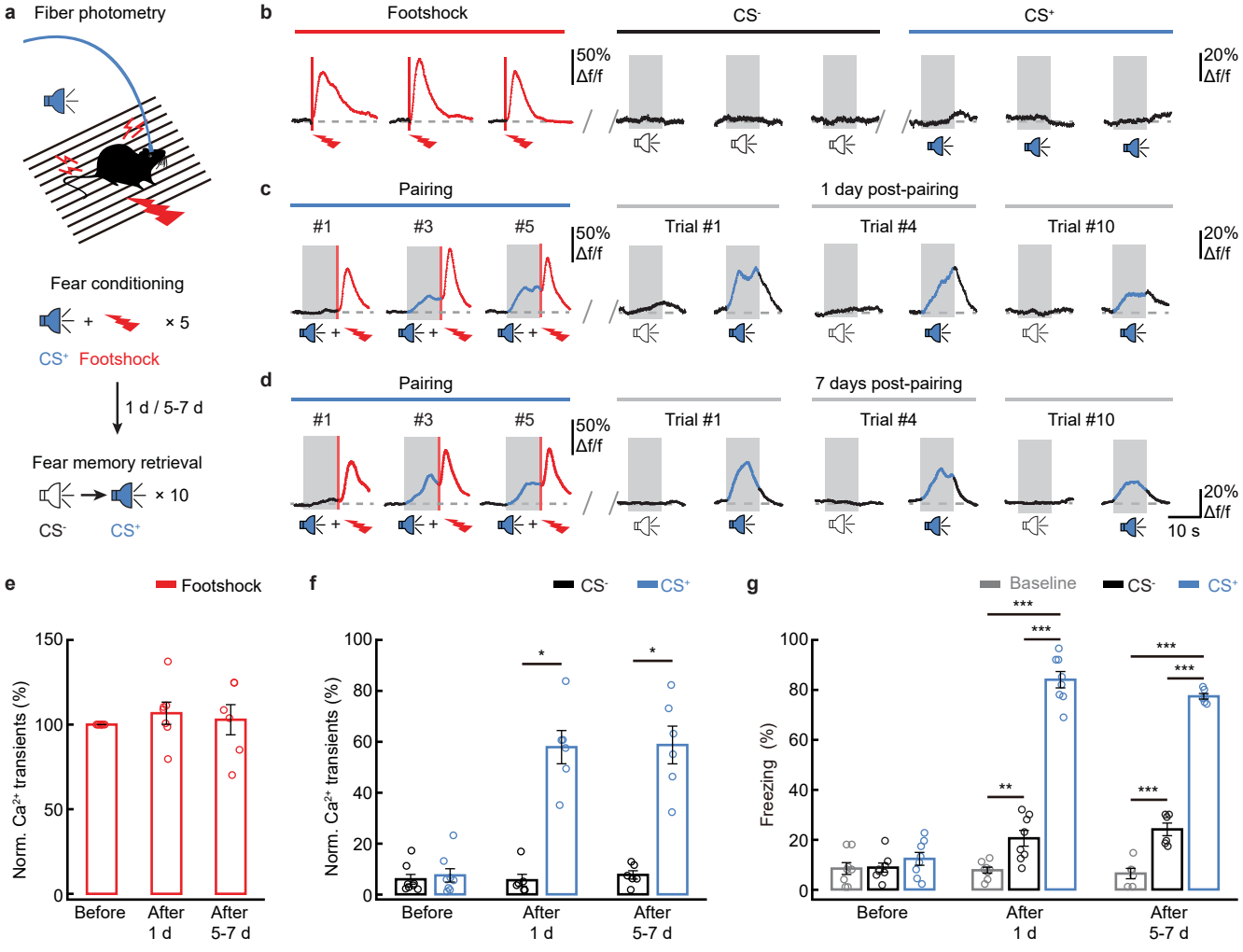
a
Fiber photometry
Fear conditioning
× 5
CS+ Footshock
1 d / 5-7 d
Fear memory retrieval
× 10
CS-
CS+
b
Footshock
CS-
CS+
50% Δf/f
20% Δf/f
c
Pairing
1 day post-pairing
#1
#3
#5
Trial #1
Trial #4
Trial #10
d
Pairing
7 days post-pairing
10 s
e
Footshock
Norm. Ca2+ transients (%)
Before
After 1 d
After 5-7 d
f
CS-
CS+
g
Baseline
Freezing (%)

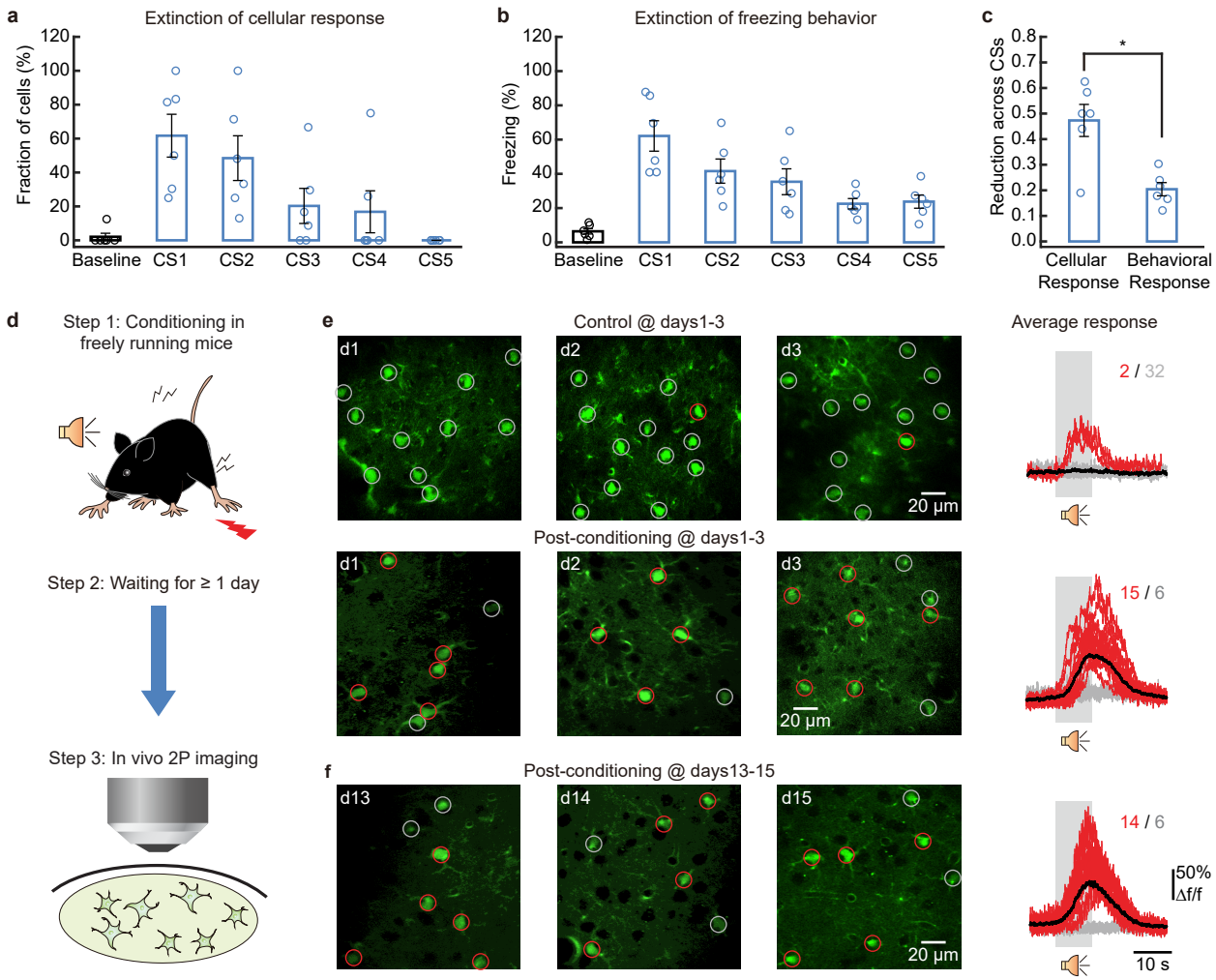
a
Extinction of cellular response
Fraction of cells (%)
Baseline
CS1
CS2
CS3
CS4
CS5
b
Extinction of freezing behavior
Freezing (%)
c
Reduction across CSs
Cellular Response
Behavioral Response
d
Step 1: Conditioning in freely running mice
Step 2: Waiting for ≥ 1 day
Step 3: In vivo 2P imaging
e
Control @ days1-3
Post-conditioning @ days1-3
Average response
2 / 32
15 / 6
f
Post-conditioning @ days13-15
14 / 6
50% Δf/f
10 s
20 μm
g
Control
Post-conditioning
Fraction of cells (%)
80 (6)
40 (7)
152 (6)
43 (6)
82 (6)
68 (6)
1-4 days
5-8 days
11-15 days
h
Post-conditioning
Extinction
i
Ca²⁺ transients (%)
j

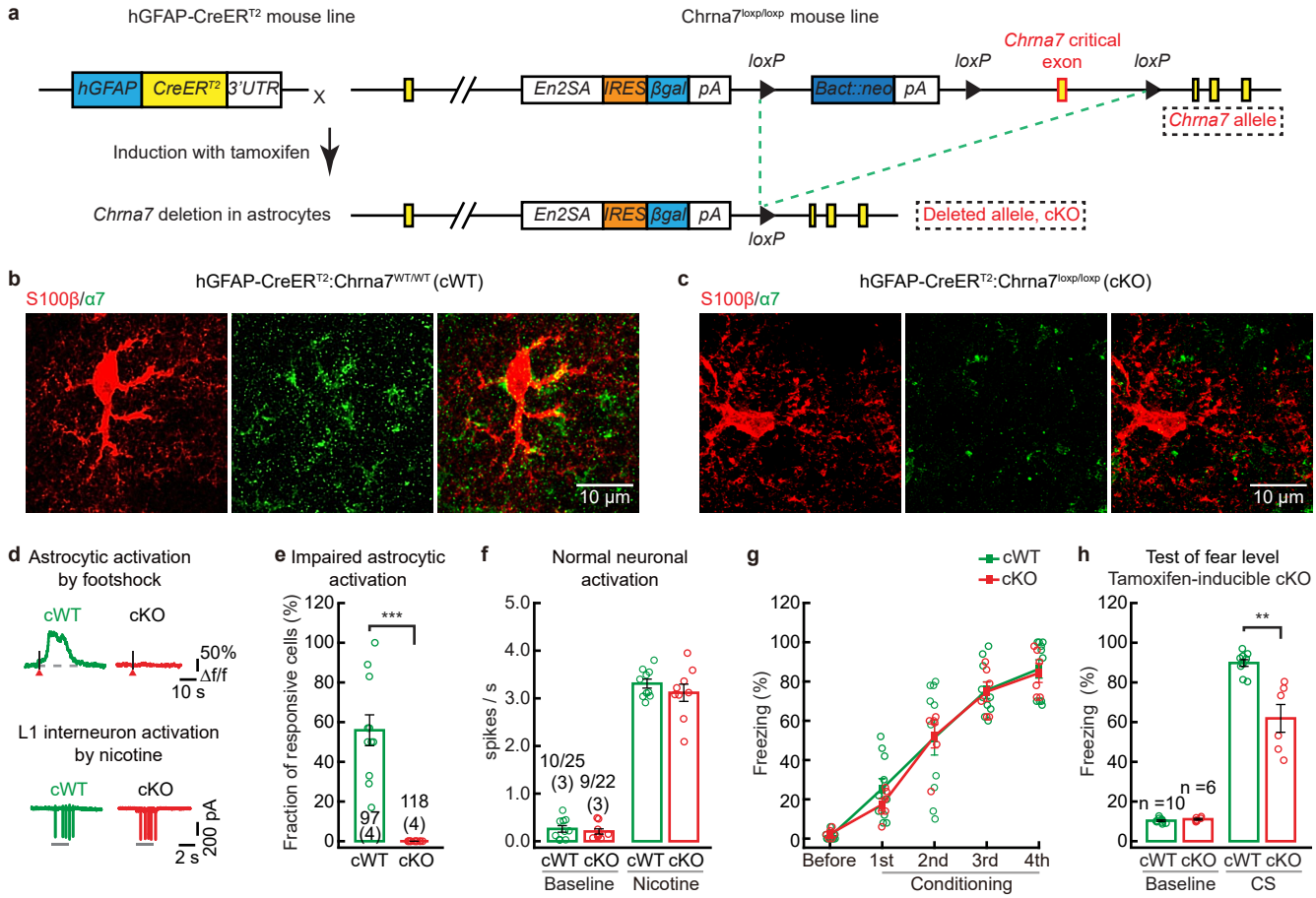
a
hGFAP-CreER$^{T2}$ mouse line
Chrna7$^{loxp/loxp}$ mouse line
hGFAP
CreER$^{T2}$
3'UTR
X
En2SA
IRES
βgal
pA
loxP
Bact::neo
pA
loxP
Chrna7 critical exon
loxP
Chrna7 allele
Induction with tamoxifen
Chrna7 deletion in astrocytes
En2SA
IRES
βgal
pA
loxP
Deleted allele, cKO
b
hGFAP-CreER$^{T2}$:Chrna7$^{WT/WT}$ (cWT)
S100β/α7
10 μm
c
hGFAP-CreER$^{T2}$:Chrna7$^{loxp/loxp}$ (cKO)
S100β/α7
10 μm
d
Astrocytic activation by footshock
cWT
cKO
50% Δf/f
10 s
L1 interneuron activation by nicotine
cWT
cKO
200 pA
2 s
e
Impaired astrocytic activation
Fraction of responsive cells (%)
***
97 (4)
118 (4)
cWT
cKO
f
Normal neuronal activation
spikes / s
10/25 (3)
9/22 (3)
cWT cKO
Baseline
cWT cKO
Nicotine
g
cWT
cKO
Freezing (%)
Before
1st
2nd
3rd
4th
Conditioning
h
Test of fear level
Tamoxifen-inducible cKO
Freezing (%)
**
n =10
n =6
cWT cKO
Baseline
cWT cKO
CS

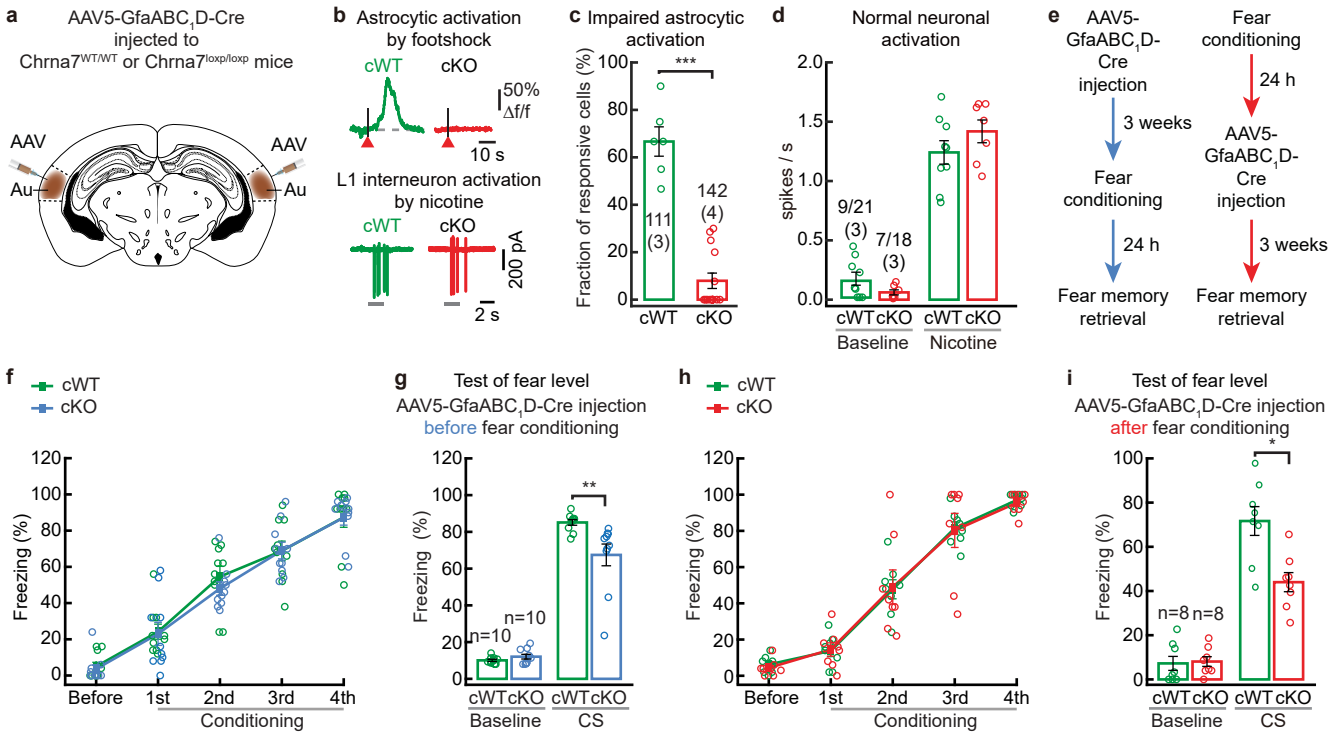
a
AAV5-GfaABC1D-Cre injected to Chrna7WT/WT or Chrna7loxp/loxp mice
AAV
Au
b
Astrocytic activation by footshock
cWT
cKO
50% Δf/f
10 s
L1 interneuron activation by nicotine
200 pA
2 s
c
Impaired astrocytic activation
Fraction of responsive cells (%)
***
111 (3)
142 (4)
d
Normal neuronal activation
spikes / s
9/21 (3)
7/18 (3)
Baseline
Nicotine
e
AAV5-GfaABC1D-Cre injection
3 weeks
Fear conditioning
24 h
Fear memory retrieval
Fear conditioning
24 h
AAV5-GfaABC1D-Cre injection
3 weeks
Fear memory retrieval
f
Freezing (%)
Before
1st
2nd
3rd
4th
Conditioning
g
Test of fear level
AAV5-GfaABC1D-Cre injection before fear conditioning
n=10
n=10
**
Baseline
CS
h
Conditioning
i
Test of fear level
AAV5-GfaABC1D-Cre injection after fear conditioning
n=8
n=8
*

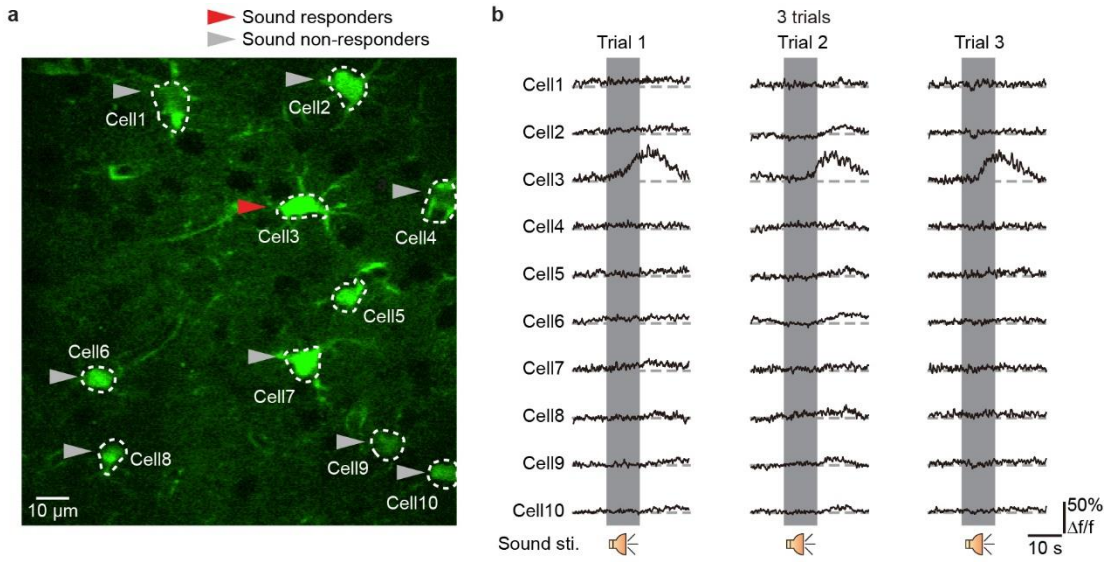


Extended Data Figure 1

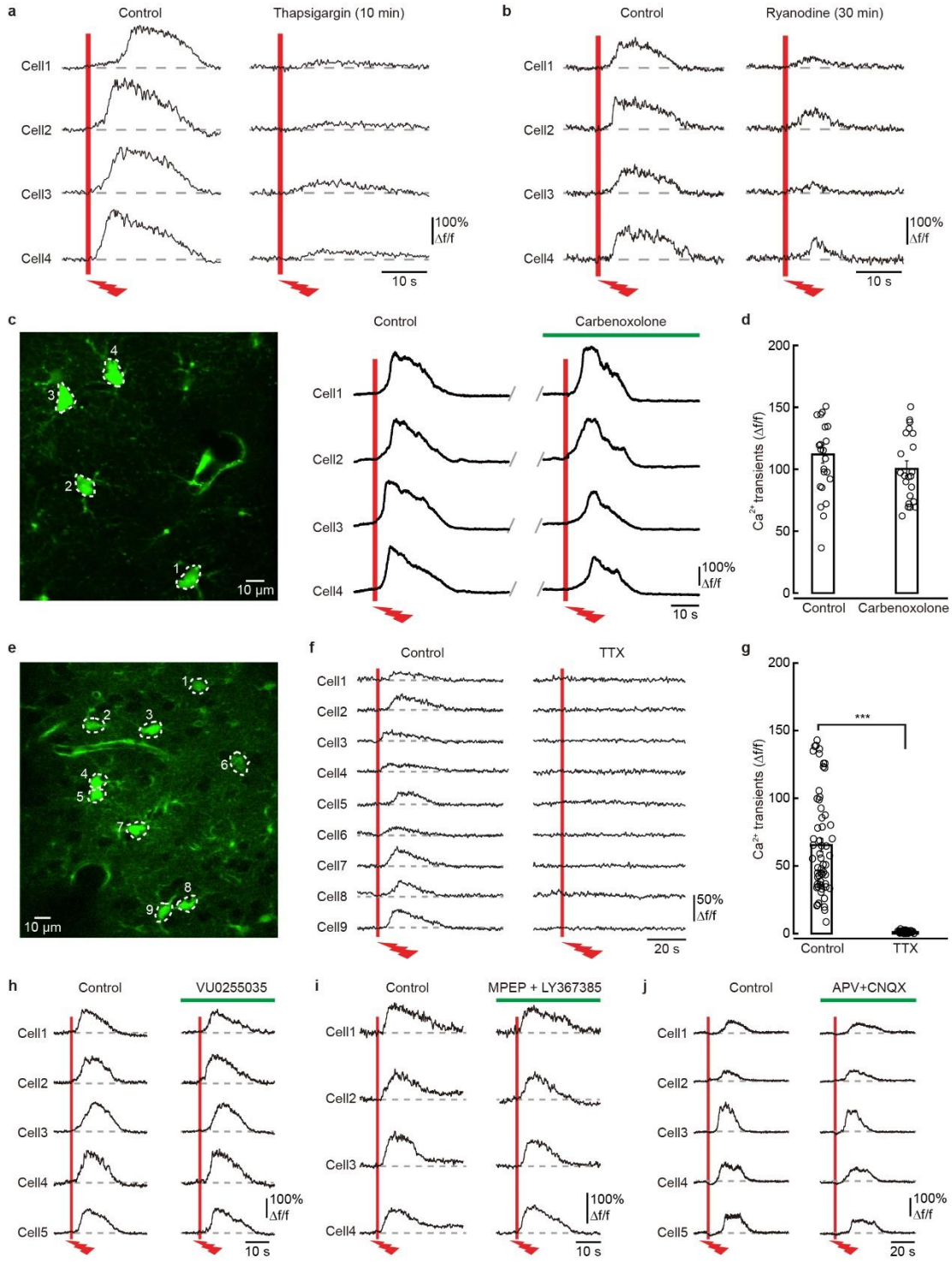


Extended Data Figure 2

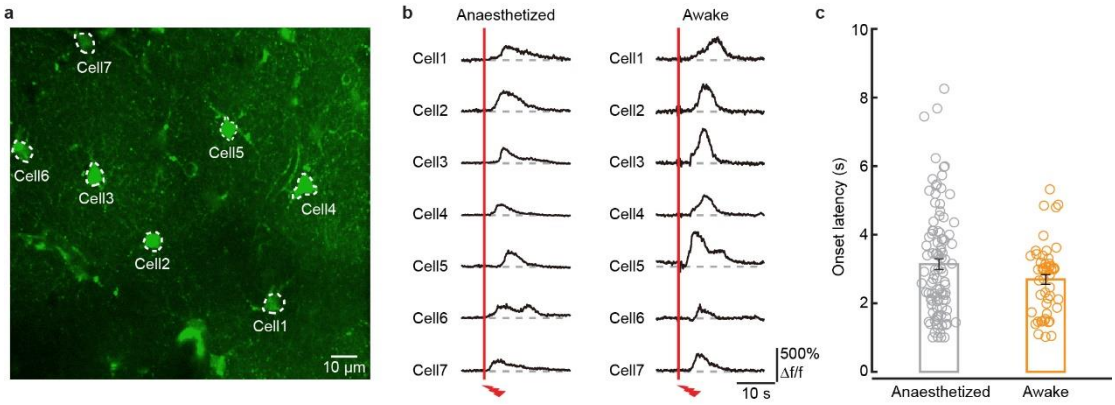


Extended Data Figure 3

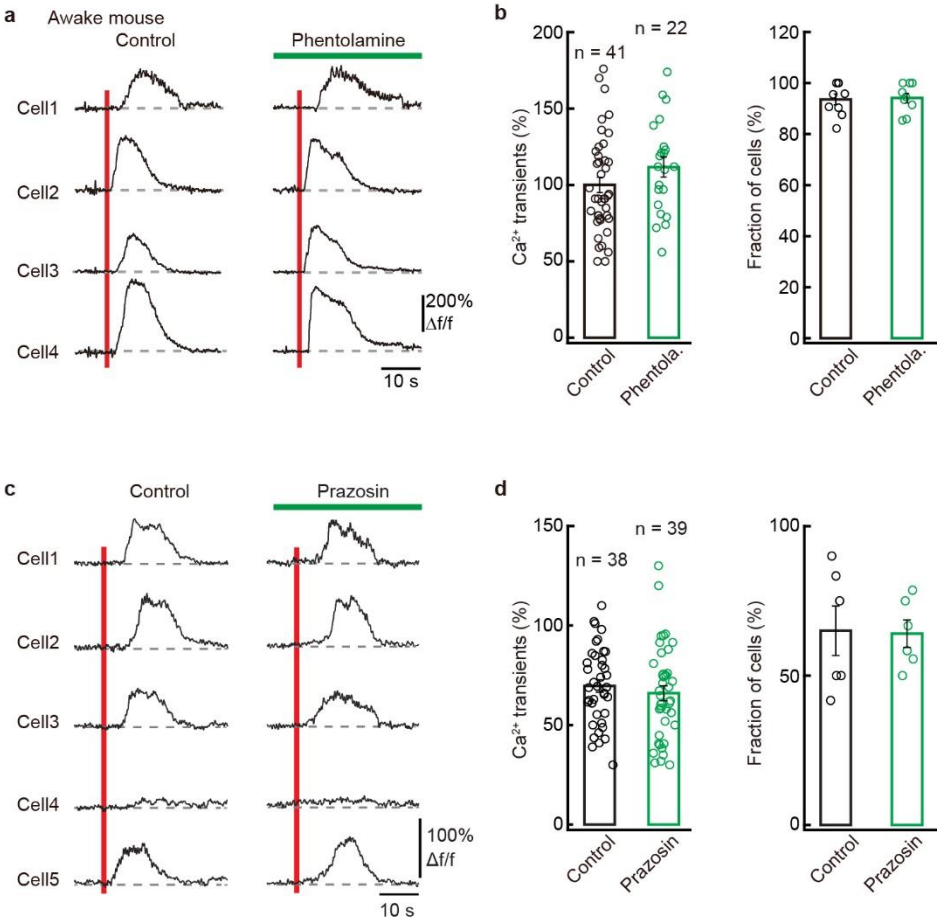


Extended Data Figure 4

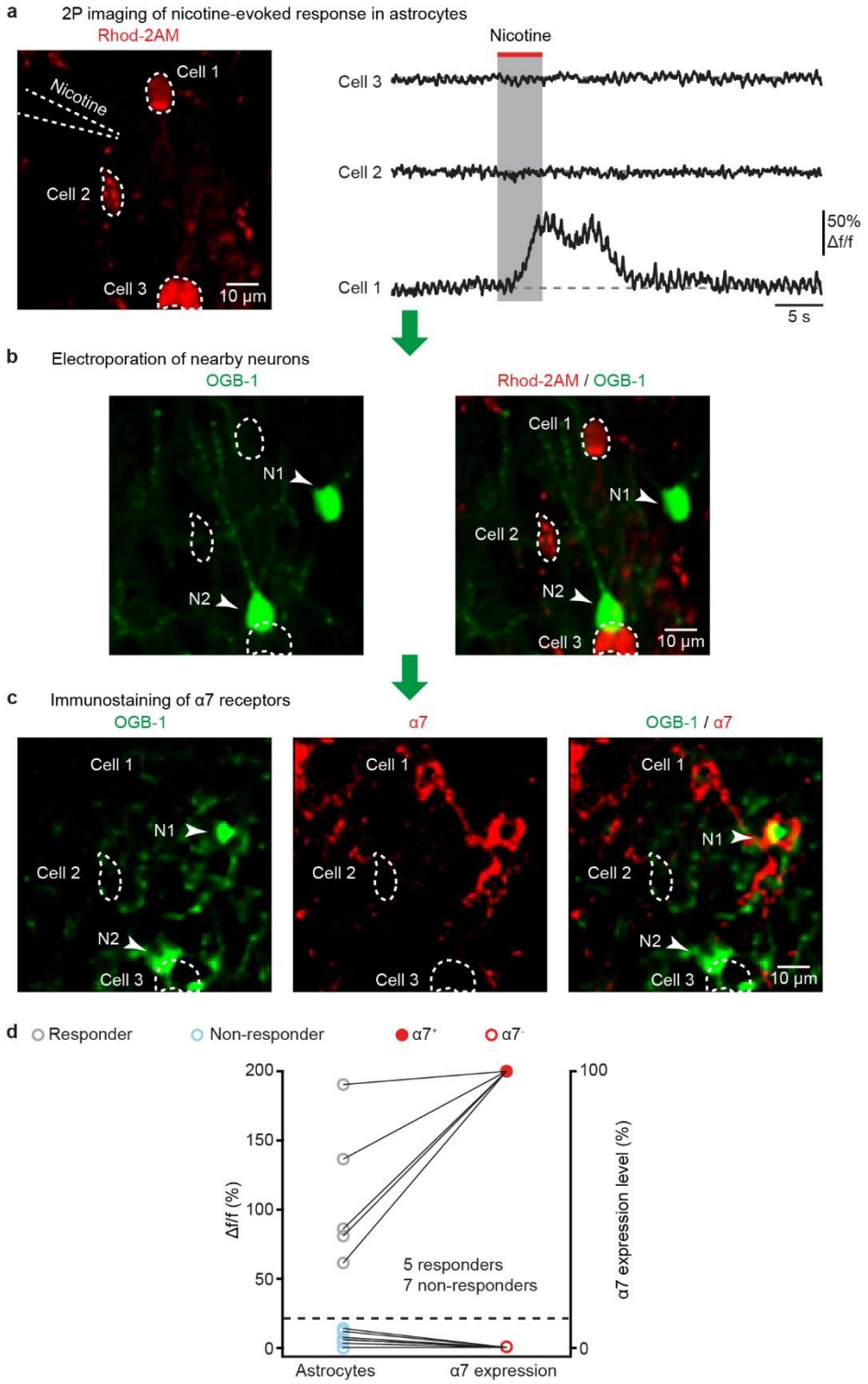


Extended Data Figure 5

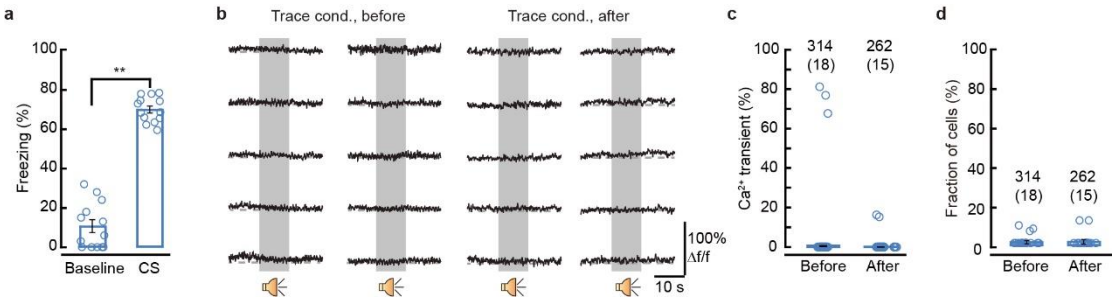


Extended Data Figure 6

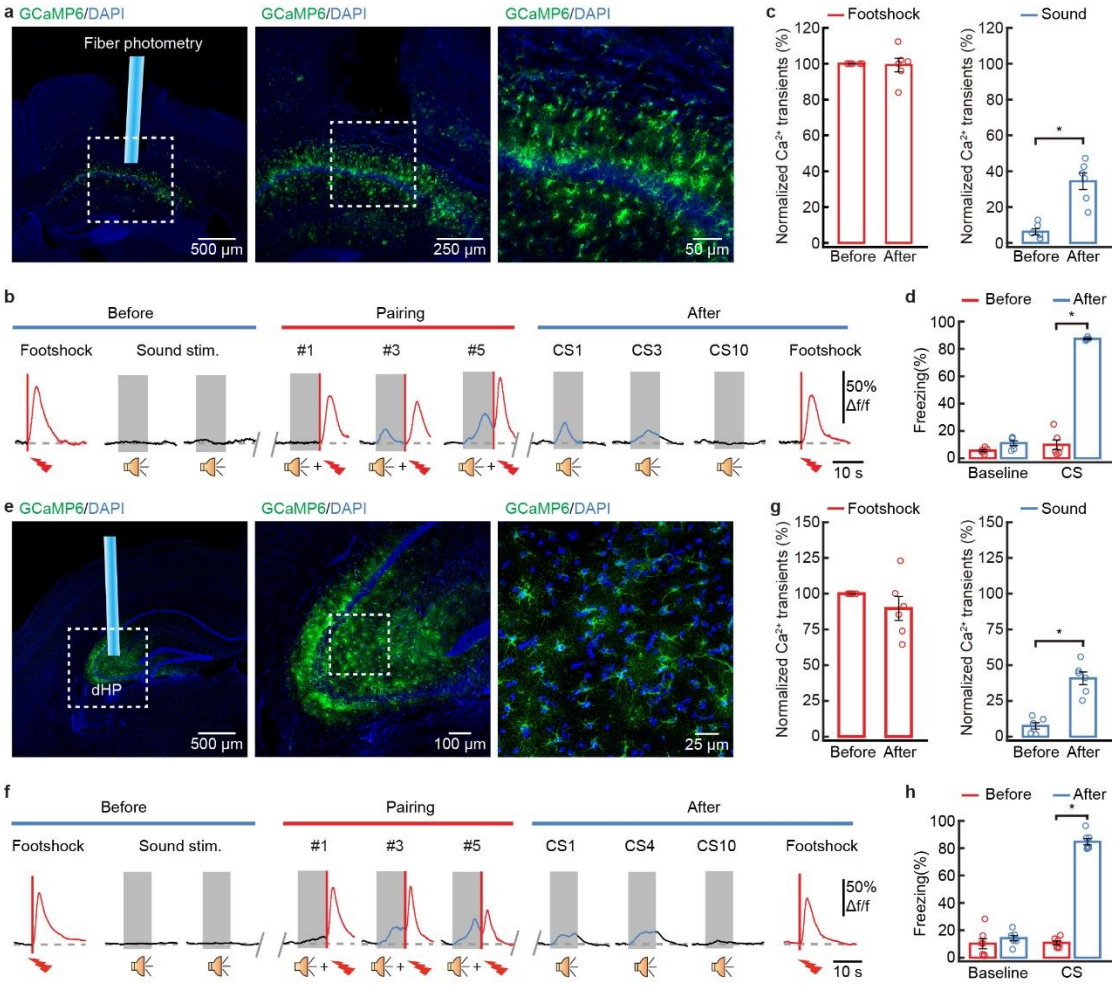


Extended Data Figure 7

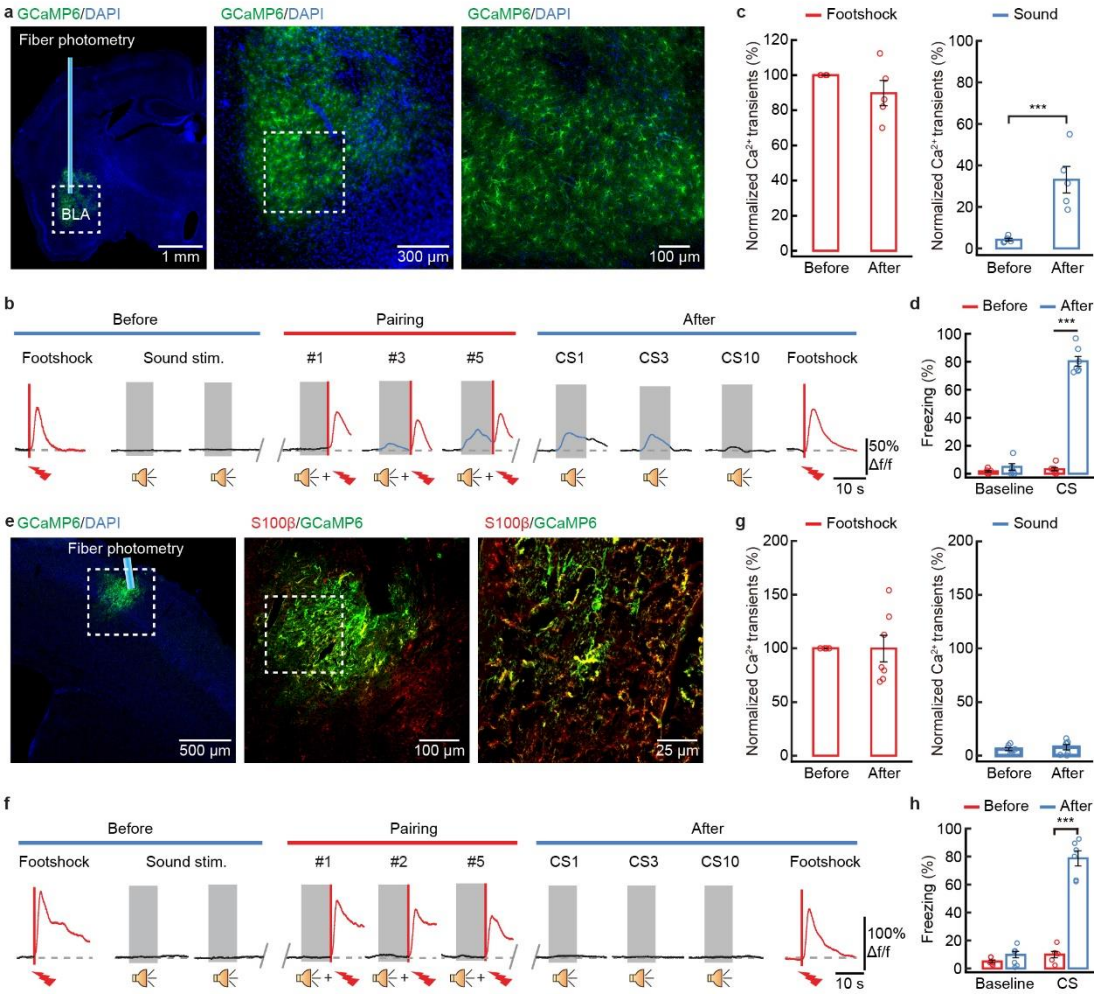


Extended Data Figure 8

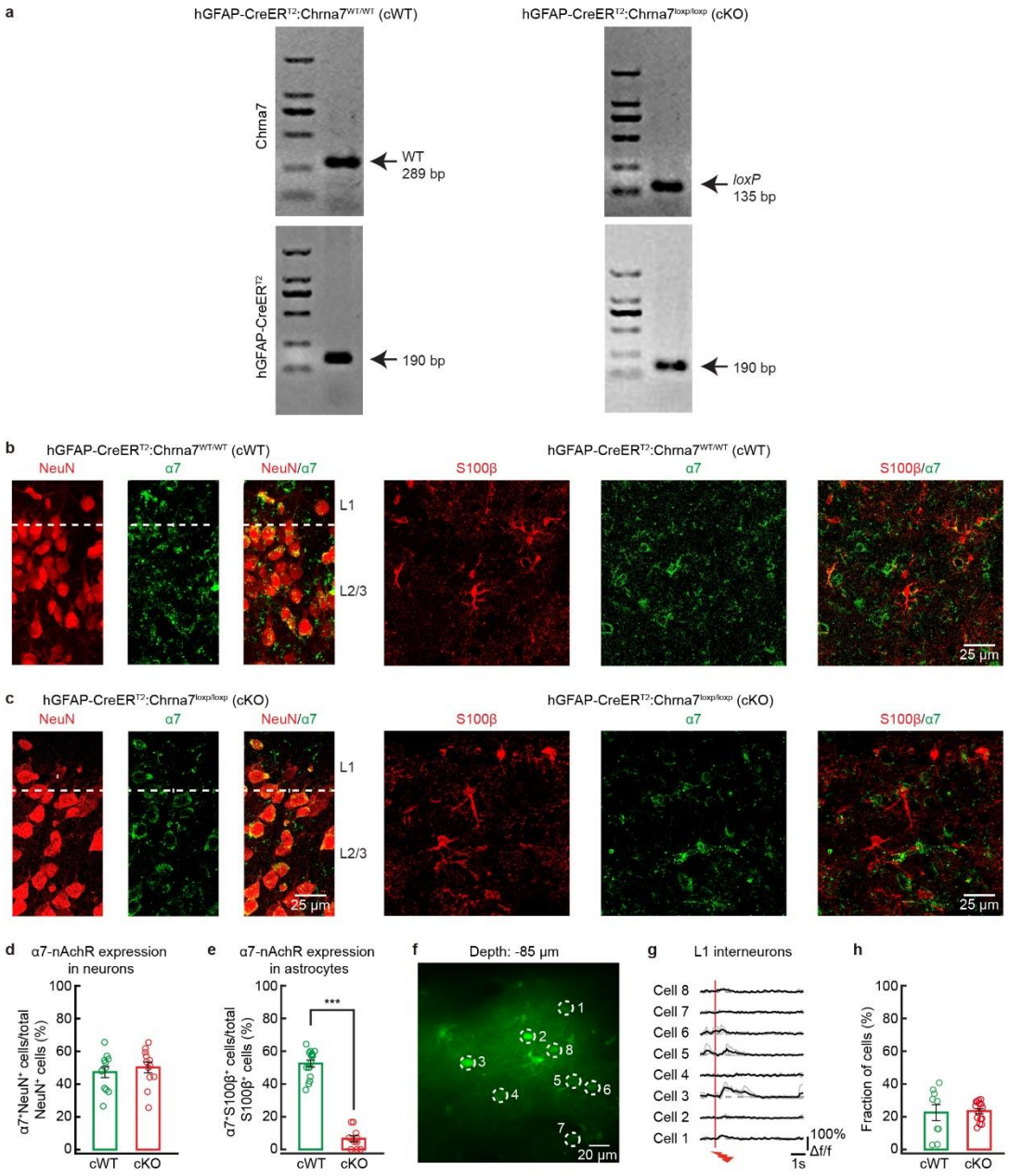


Extended Data Figure 9

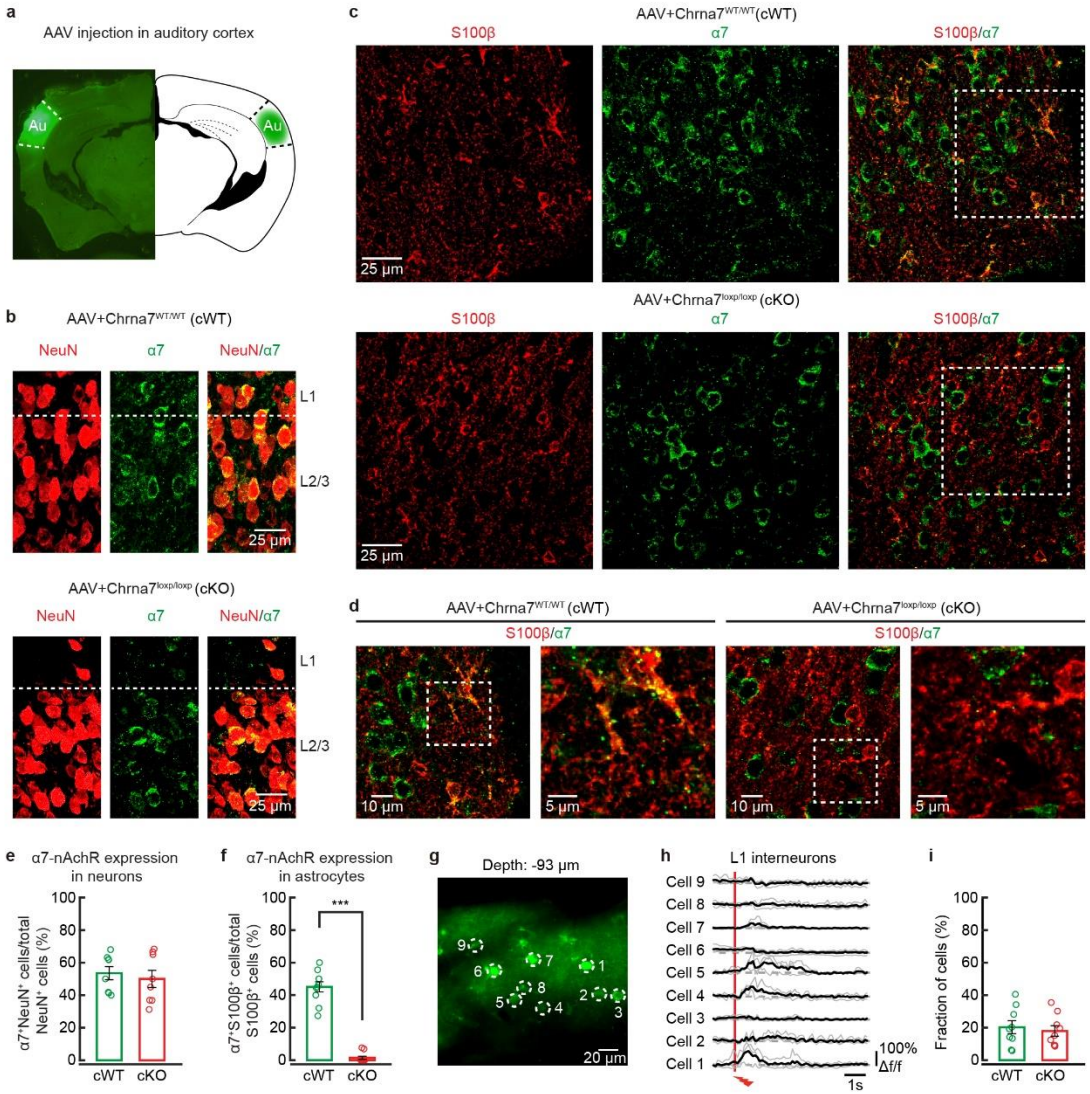


Extended Data Figure 10